

Compact magneto-optical traps using planar optics

Zhi Tan(谭智), Bo Lu(鹿博), Chengyin Han(韩成银), and Chaohong Lee(李朝红)

Citation: Chin. Phys. B, 2024, 33 (**9**): 093701. DOI: 10.1088/1674-1056/ad607a
Journal homepage: http://cpb.iphy.ac.cn; http://iopscience.iop.org/cpb

What follows is a list of articles you may be interested in

Enhanced cold mercury atom production with two-dimensional magneto-optical trap

Ye Zhang(张晔), Qi-Xin Liu(刘琪鑫), Jian-Fang Sun(孙剑芳), Zhen Xu(徐震), and Yu-Zhu Wang(王育竹)
Chin. Phys. B, 2022, 31 (**7**): 073701. DOI: 10.1088/1674-1056/ac5397

Optimization of a magneto-optic trap using nanofibers

Xin Wang(王鑫), Li-Jun Song(宋丽军), Chen-Xi Wang(王晨曦), Peng-Fei Zhang(张鹏飞), Gang Li(李刚), Tian-Cai Zhang(张天才)
Chin. Phys. B, 2019, 28 (**7**): 073701. DOI: 10.1088/1674-1056/28/7/073701

Loss of cold atoms due to collisions with residual gases in free flight and in a magneto-optical trap

Jing-feng Xiang(项静峰), He-nan Cheng(程鹤楠), Xiang-kai Peng(彭向凯), Xin-wen Wang(王新文), Wei Ren(任伟), Jing-wei Ji(吉经纬), Kang-kang Liu(刘亢亢), Jian-bo Zhao(赵剑波), Lin Li(李琳), Qiu-zhi Qu(屈求智), Tang Li(李唐), Bin Wang(汪斌), Mei-feng Ye(叶美凤), Xin Zhao(赵鑫), Yuan-yuan Yao(姚媛媛), De-Sheng Lü(吕德胜), Liang Liu(刘亮)
Chin. Phys. B, 2018, 27 (**7**): 073701. DOI: 10.1088/1674-1056/27/7/073701

Highly sensitive photoassociation spectroscopy of ultracold $^{23}Na^{133}Cs$ molecular long-range states below the $3S_{1/2}+6P_{3/2}$ limit

Yanyan Liu(刘艳艳), Jizhou Wu(武寄洲), Wenliang Liu(刘文良), Xiaofeng Wang(王晓锋), Wenhao Wang(王文浩), Jie Ma(马杰), Liantuan Xiao(肖连团), Suotang Jia(贾锁堂)
Chin. Phys. B, 2017, 26 (**12**): 123702. DOI: 10.1088/1674-1056/26/12/123702

Intense source of cold cesium atoms based on a two-dimensional magneto-optical trap with independent axial cooling and pushing

Jia-Qiang Huang(黄家强), Xue-Shu Yan(颜学术), Chen-Fei Wu(吴晨菲), Jian-Wei Zhang(张建伟), Li-Jun Wang(王力军)
Chin. Phys. B, 2016, 25 (**6**): 063701. DOI: 10.1088/1674-1056/25/6/063701

TOPICAL REVIEW — Quantum computing and quantum sensing

Compact magneto-optical traps using planar optics

Zhi Tan(谭智)[1], Bo Lu(鹿博)[1,2], Chengyin Han(韩成银)[1,2,†], and Chaohong Lee(李朝红)[1,2,‡]

[1] *Institute of Quantum Precision Measurement, State Key Laboratory of Radio Frequency Heterogeneous Integration, College of Physics and Optoelectronic Engineering, Shenzhen University, Shenzhen* 518060, *China*

[2] *Quantum Science Center of Guangdong–Hong Kong–Macao Greater Bay Area (Guangdong), Shenzhen* 518045, *China*

(Received 6 May 2024; revised manuscript received 5 July 2024; accepted manuscript online 9 July 2024)

Magneto-optical traps (MOTs) composed of magnetic fields and light fields have been widely utilized to cool and confine microscopic particles. Practical technology applications require miniaturized MOTs. The advancement of planar optics has promoted the development of compact MOTs. In this article, we review the development of compact MOTs based on planar optics. First, we introduce the standard MOTs. We then introduce the grating MOTs with micron structures, which have been used to build cold atomic clocks, cold atomic interferometers, and ultra-cold sources. Further, we introduce the integrated MOTs based on nano-scale metasurfaces. These new compact MOTs greatly reduce volume and power consumption, and provide new opportunities for fundamental research and practical applications.

Keywords: magneto-optical trap (MOT), planar optics, grating MOT, metasurface MOT

PACS: 37.10.–x, 37.10.De, 42.62.Eh **DOI:** 10.1088/1674-1056/ad607a

1. Introduction

The magneto-optical trap (MOT), combining the abilities of cooling and trapping atoms, has become a workhorse in the field of laser cooling. Since the 1980s, the MOT has evolved from a theoretical concept[1,2] to a widely used cooling technique.[3–12] The atoms in MOT can be cooled to temperatures close to absolute zero, enabling the study of the properties of matter at extremely low kinetic energies. Currently, the MOT has made significant progress in the laser cooling and trapping of atoms and molecules.[13–23] The species of atoms under study include not only alkali metals (such as lithium,[24–26] sodium,[27–30] potassium,[31–34] rubidium,[35–40] caesium,[41–49] and francium[50,51]) but also alkaline earth and earth-like metals (such as magnesium,[52–54] calcium,[55,56] strontium,[55,57] ytterbium,[58–61] and mercury[62–65]) as well as inert gases (such as helium,[66,67] neon,[68] argon,[69] krypton,[69] xenon[70]) and so on.[71–78] Meanwhile, cold atoms are widely applied in the field of quantum technologies,[79,80] including high-precision atomic clocks,[81–98] high-sensitivity magnetometers,[99–111] atomic interferometers,[112–129] electromagnetic field sensors,[130] vacuum sensors,[131] quantum simulations,[132–142] quantum computers,[143–147] quantum networks,[148] and quantum memories.[149–152]

The practical application of atomic quantum sensors requires miniaturized MOT. The traditional MOT systems possess unique optical setups, utilizing three pairs of counter-propagating laser beams with orthogonal polarization and red detuning in combination with a quadrupole magnetic field to provide spatial confinement. The traditional MOT offers outstanding performance in cold atom trapping, but is bulky and not conducive to applications in compact spaces.[153] Planar optics can significantly reduce the size of the experimental setup. Therefore, how to prepare cold atoms in a convenient and effective way has become an attractive topic.

Over the past two decades, efforts to miniaturize MOTs[154–164] have led to the emergence of many different types of them. Among them, integrated MOTs based on planar optics are developing rapidly, especially the grating magneto-optical trap (GMOT). The GMOT utilizes an incident laser beam to produce secondary beams on a set of gratings,[165] combining these beams together with an appropriate quadrupole magnetic field to form a MOT above the gratings. The GMOT can simplify the optical system to a single laser beam input, which greatly reduces volume and power consumption and has been used to produce Bose–Einstein condensate (BEC).[166] Combined with atom chips, GMOT may play an important role in the evaporative cooling process of BECs. Another exciting technique in planar optics is the integrated device based on metasurface,[167–175] which consists of subwavelength structures with spatially varying properties, offering the capability to control amplitude, polarization, and phase.[176–183] This integrated device greatly reduces the size of the system while enriching the degrees of freedom for light field modulation. The planar optics open up new possibilities for the development of integrated MOT.

Stimulated by the promising applications of compact MOTs, this article aims to provide an overview of compact

†Corresponding author. E-mail: hanchy@szu.edu.cn

‡Corresponding author. E-mail: chleecn@szu.edu.cn

© 2024 Chinese Physical Society and IOP Publishing Ltd

MOTs using planar optics. Firstly, the basic principles of standard MOT are introduced, and the MOT with plane magnetic wire is described in Section 2. Then, the principles of GMOTs are described in detail, and the performance of different kinds of GMOTs is compared in Section 3. Additionally, we introduce the principle of metasurface-based MOTs in Section 4. Finally, brief summary and outlook are provided in Section 5.

2. Magneto-optical trap

In this section, we will introduce the principle of standard MOTs. We start from the basic principle of standard MOTs, which are also known as the conventional MOTs. We also mention the MOT with planar magnetic wire.

2.1. Standard magneto-optical trap

The standard MOT is a device that utilizes a combination of laser and magnetic fields technology to achieve the cooling, trapping and manipulating of neutral atoms or molecules, as shown in Fig. 1(a).[184] In general, the magnetic trap of standard MOT essentially consists of a pair of coils with the same current amplitude and opposite directions, as the label $\pm\boldsymbol{I}$ in Fig. 1(a). Such a set of anti-Helmholtz coils perpendicular to the z axis generates a quadrupole magnetic field in the space. According to the Biot–Savart law, the magnetic field from the anti-Helmholtz coil is obtained by integrating over each element on the coils.[185] The result is displayed in Fig. 1(b), the blue arrows indicate the direction of the magnetic field, and the length of the arrows denotes the strength of the magnetic field. The magnetic field strength is zero at the origin of the coordinates and increases linearly from the center to the edges in the spatial of MOT. The Maxwell equation $\nabla\cdot\boldsymbol{B}=0$ implies that $\boldsymbol{B}=A(x\boldsymbol{e}_x+y\boldsymbol{e}_y-2z\boldsymbol{e}_z)$, the magnitude of the magnetic field $B=|\boldsymbol{B}|=A(x^2+y^2+4z^2)^{1/2}$, and the gradient in any radial direction is half of that along the z-direction.

The realization of the MOT requires the atoms to have a magnetic dipole. Assuming the ground state of the atom has a total angular momentum $J=0$, the Zeeman displacements of the three sub-levels vary with the strength of the magnetic field, as the black line shown in Fig. 1(d). Then the magnetic dipole $\boldsymbol{\mu}$ in an external magnetic field $\boldsymbol{B}$ has energy $U=-\boldsymbol{\mu}\cdot\boldsymbol{B}=-\mu|\boldsymbol{B}|\cos\theta$, which denotes the rapid motion of the magnetic moment $\boldsymbol{\mu}$ around the magnetic field with a constant angle θ. When near the center point, the magnetic field can be written as $B=A(r^2+4z^2)^{1/2}\approx A(r^2+4z^2)$, so the atoms of mass M see a harmonic potential

$$U(r,z)=-\left(\frac{1}{2}M\omega_r^2r^2+\frac{1}{2}M\omega_z^2z^2\right), \tag{1}$$

where $r=\sqrt{x^2+y^2}$ is the radial coordinate, ω_r^2 and ω_z^2 are the radial and axial angular frequencies. In quantum mechanics, for an atom in the sate $|J,m_J\rangle$, the energy corresponds to a Zeeman energy $U=-g_J\mu_{\rm B}m_J|\boldsymbol{B}|$, g_J represents the Landé factor. This energy does not vary with the direction of $\boldsymbol{B}$ and only depends on the magnitude of the field B. This is because when the dipole moves adiabatically, it stays aligned with the field. Then one can induce the magnetic force along z-direction

$$F_B=-\nabla U=g_J\mu_{\rm B}m_J\frac{{\rm d}B}{{\rm d}z}, \tag{2}$$

which is related to atomic ground states, excited states, hyperfine energy levels, and Zeeman energy levels.

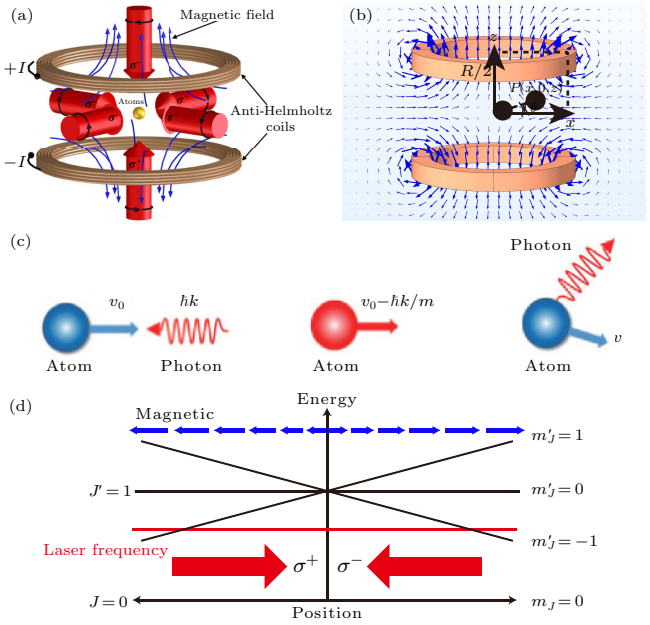


Fig. 1. (a) The schematic of a standard MOT. The blue line represents the direction of the magnetic field.[184] (b) The magnetic field distribution of the anti-Helmholtz coil in xoz plane simulated by COMSOL simulation software. The point P in the figure represents any field point in the xoz plane, and θ denotes the angle between the field point and the x-axis. (c) The schematic of the force on absorbing and spontaneously radiating photon of atom. An atom with velocity v_0 encounters a photon with momentum $\hbar k$, after absorbing the photon, the atom re-radiation in a random direction. (d) The energy levels of atoms along the horizontal direction. It shows the Zeeman splitting of magnetic sublevels of $J=0\rightarrow J'=1$ in the presence of a quadrupole magnetic field.

The laser cooling in the MOT origins from the mechanical force of the light field on the atoms, which reduces the kinetic energy of the atoms.[186] The force of a light field on an atom consists of two parts, which are respectively proportional to the amplitude gradient and phase gradient of the optical field

$$\boldsymbol{F}=\boldsymbol{F}_{\rm dipole}+\boldsymbol{F}_{\rm scatt}=\frac{\hbar\Omega}{2}\left(u\frac{\nabla\Omega}{\Omega}+v\nabla\phi\right), \tag{3}$$

where u, v are time-dependent parameters in optical Bloch equation, Ω is the Rabi frequency, ϕ is coordinate-dependent phase factor. Since the light field in the MOT is collimated and nearly resonant, there is no dipole force in the MOT.

To understand the scattering force, we start from a single atom. The schematic diagram of an atom cooled by photon

is shown in Fig. 1(c). After the atom absorbs the photon, the velocity is reduced by $\hbar k/m$, where m is the mass of the atom. The atom stays in the excited state for a while and then spontaneously radiates a photon in a random direction. By repeating this process, the average velocity of the atom gradually decreases, achieving the purpose of cooling. The energy of the atoms and light field system is continuously dissipated into the spontaneous radiation field (e.g., vacuum field) by absorbing photons. This process involves scattering of the light field, and therefore, the force exerted on the atoms is commonly referred to as the scattering force, known as radiation pressure. The scattering force equals the rate at which the absorbed photons impart momentum to the atom, so that

$$\begin{aligned} \boldsymbol{F}_{\text{scatt}} &= \hbar\boldsymbol{k}\cdot\boldsymbol{R}_{\text{scatt}} \\ &= \hbar\boldsymbol{k}\cdot\frac{\Gamma}{2}\frac{I/I_{\text{sat}}}{1+I/I_{\text{sat}}+4(\omega-\omega_0+\boldsymbol{k}\cdot\boldsymbol{v})^2/\Gamma^2}. \end{aligned} \tag{4}$$

where I_{sat} is the saturation intensity, $I/I_{\text{sat}}=2\Omega^2/\Gamma^2$, Γ is the natural linewidth. The frequency detuning from resonance is the difference between the laser frequency ω and the atomic resonance frequency ω_0 taking into account the Doppler shift kv.

The optical field in a standard MOT consists of three pairs of mutually perpendicular laser beams with circular polarization and red detuning. It can make atoms with speed below a certain value stably trapped in the laser crossing point. Taking z-axis in Fig. 1(d) as an example, there is a pair of counter-propagating laser beams of the same intensity along the z-axis with polarization directions of σ^+ and σ^-. The atoms moving in the region of $z>0$ would absorb more photons of σ^- and be excited to the upper energy level state of $m_J'=-1$. This is due to the fact that the laser frequency is closer to the transition of $\Delta m_J'=-1$ where the detuning is smaller, leading to a negative force towards the trap center. While the reverse is true for the $z<0$ condition. Thereby the radiation pressure is applied to all atoms pointing to the origin of the coordinates, which is similar to the force applied to atoms in a parabolic potential. It is possible to obtain similar results for the other directions, thus realizing the three-dimensional confinement of atoms. The radiation pressure on the atoms in the standard MOT is written as

$$\begin{aligned} \boldsymbol{F}_{\text{MOT}} &= \boldsymbol{F}_{\text{scatt}}^{\sigma^+}\Big(\omega-\boldsymbol{k}\cdot\boldsymbol{v}-(\omega_0+\boldsymbol{\beta}\cdot\boldsymbol{r})\Big)+\boldsymbol{F}_{\text{scatt}}^{\sigma^-}\Big(\omega+\boldsymbol{k}\cdot\boldsymbol{v}-(\omega_0-\boldsymbol{\beta}\cdot\boldsymbol{r})\Big) \\ &= \hbar k\frac{\Gamma}{2}\left(\frac{I/I_{\text{sat}}}{1+I/I_{\text{sat}}+4(\frac{\omega-\boldsymbol{k}\cdot\boldsymbol{v}-(\omega_0+\boldsymbol{\beta}\cdot\boldsymbol{r})}{\Gamma})^2}-\frac{I/I_{\text{sat}}}{1+I/I_{\text{sat}}+4(\frac{\omega+\boldsymbol{k}\cdot\boldsymbol{v}-(\omega_0-\boldsymbol{\beta}\cdot\boldsymbol{r})}{\Gamma})^2}\right)\simeq -2\frac{\partial\boldsymbol{F}}{\partial\omega}\cdot\boldsymbol{k}\cdot\boldsymbol{v}+2\frac{\partial\boldsymbol{F}}{\partial\omega_0}\cdot\boldsymbol{\beta}\cdot\boldsymbol{r}, \end{aligned} \tag{5}$$

where the term $\omega_0\pm\boldsymbol{\beta}\cdot\boldsymbol{r}$ is the resonant absorption frequency for the $m_J'\pm1$ transition at position $\boldsymbol{r}$, respectively. And the Zeeman shift at displacement $\boldsymbol{r}$ is

$$\boldsymbol{\beta}\cdot\boldsymbol{r}=\frac{(g_{J'}m_{J'}-g_Jm_J)\mu_{\text{B}}}{\hbar}\frac{\mathrm{d}\boldsymbol{B}}{\mathrm{d}\boldsymbol{r}}\cdot\boldsymbol{r}.$$

Since the force depends on the frequency detuning $\delta=\omega-\omega_0$, we get $\partial\boldsymbol{F}/\partial\omega_0=-\partial\boldsymbol{F}/\partial\omega$ and hence

$$\boldsymbol{F}_{\text{MOT}}=-2\frac{\partial\boldsymbol{F}}{\partial\omega}\cdot(\boldsymbol{k}\cdot\boldsymbol{v}+\boldsymbol{\beta}\cdot\boldsymbol{r})=-\alpha\boldsymbol{v}-\kappa\boldsymbol{r}, \tag{6}$$

where α is the damping coefficient of the deceleration damping force on the atoms in the light field, κ denotes the coefficient of elasticity for the atom in the potential field. Both forces cool and confine the atoms in the center of the MOT.

The design of the magnetic field and light field in standard MOT is quite flexible. For the magnetic field, different coils can be designed to adjust the shape of the magnetic field, and the strength of the magnetic field can be changed by adjusting the current in the coils. For the laser field, the beam shape, intensity, polarization and other parameters can be adjusted according to the experimental requirements to achieve the manipulation of different types of microscopic particles. However, standard MOT requires a more complex laser system and precision control of the magnetic field, which may limit the applications out of laboratory. Therefore, how to simplify the standard MOT system becomes a key issue.

2.2. Magneto-optical trap with planar wire

In response to the challenge of the large size of standard MOTs, researchers are actively exploring the implementation of planar magnetic wire[187] as a solution to achieve a more compact and versatile atomic manipulation system. The planar magnetic trap is a device that uses a magnetic field to form a stable potential in three-dimensional space. The key to this scheme lies in the design of special magnetic field structures that generate magnetic fields with specific shapes and strengths, thus enabling atoms to be confined to specific regions. In this way, not only the system volume can be reduced, but also the flexibility and integrability of the system can be improved, providing broader possibilities for research in the field of cold atom physics and quantum information.

The concept of planar magnetic traps was initially employed in schemes for atom guiding, which refers to the controlled transport of a group of atoms from one position to another along specially planned trajectories.[188] Based on current-carrying straight wires, a variety of micromag-

netic traps similar to quadrupole and Ioffe–Pritchard traps can be constructed by bending wires.[189–196] In the top row of Fig. 2(a), it is displayed that a wire has been bent in the U shape. The currents in the two arms of the U-shaped wire are in opposite directions. After adding a uniform bias magnetic field, it is possible to find a position where the magnetic field intensities cancel each other completely. Therefore, there is always a zero point present in the trap potential. The horizontal and vertical magnetic potentials are shown in the right column of Fig. 2(a). If the bias magnetic field was parallel to the bent wire, a magnetic trap similar to a quadrupole trap would be formed. Another way of bending is to construct the Z-shaped wire, as shown in the bottom row of Fig. 2(a). The direction of current is the same in both arms of the Z-shaped wire, and it is clear that the Z-shaped wire has no magnetic field zero point. The position of the lowest point of the magnetic field is directly above or below the Z-shaped wire, which is an anti-parabolic shaped potential. This configuration creates the Ioffe–Pritchard trap when the bias magnetic field is applied parallel to the wire. Therefore, this magnetic trap can effectively avoid the Majorana transition.

Subsequently different types of MOTs with magnetic wire have been realized in experiments. In 1999, the group of Haase[192] experimentally realized the Z-shaped wire and investigated its properties by using cold lithium atoms. They bent a standard 1 mm thick copper wire into Z-shape as shown in Fig. 2(b). The center wire of the Z-shaped wire is 6 mm long, the arms of the wire are 25 mm long, and the wire carries a current of 25 A. The cold lithium atom cloud is located a few millimeters above the Z-shaped wire. After the measurement, the Z-shaped wire traps about $N = 3 \times 10^7$ cold lithium atoms with a collision rate of 6 s^{-1}. Besides, the idea of using crossed wires to trap atoms has been proposed, Fig. 2(c).[193] By increasing the number of wires in a certain direction, or by changing the size of the circuits in the wires, more complex magnetic traps can be constructed to trap atoms. In addition, a recent work has shown that a U-shaped wire MOT combined with an atom-chip can effectively trap cold rubidium atoms in a high-vacuum environment, as shown in Fig. 2(d).[197] The maximum number of cold atoms that can be trapped is up to 6×10^7, the number of cold rubidium atoms trapped has been raised by an order of magnitude compared to earlier studies.

Combining the planar wire magnetic trap with the light field, the MOT has a more compact structure, occupying less space. It is suitable for situations where space is limited, such as practical applications. Due to the high flexibility of planar wire magnetic trap, the magnetic field distribution can be precisely controlled by designing the layout of the wires. Additionally, the planar wire MOT can be integrated with other manipulation techniques, such as atom guide,[188,191,194,198,199] atomic motor,[189] waveguide[200,201] etc. However, in the practical application, the uniformity of planar magnetic trap may be restricted by the layout of the wires, requiring precise design and optimization to improve magnetic field uniformity. Furthermore, the planar magnetic trap requires a large external current source to drive the wires to generate the magnetic field, resulting in significant thermal power. In summary, the planar magnetic trap has advantages such as compactness and flexibility, but there are still challenges in terms of magnetic field uniformity, thermal power, and so on, which require further research and optimization.

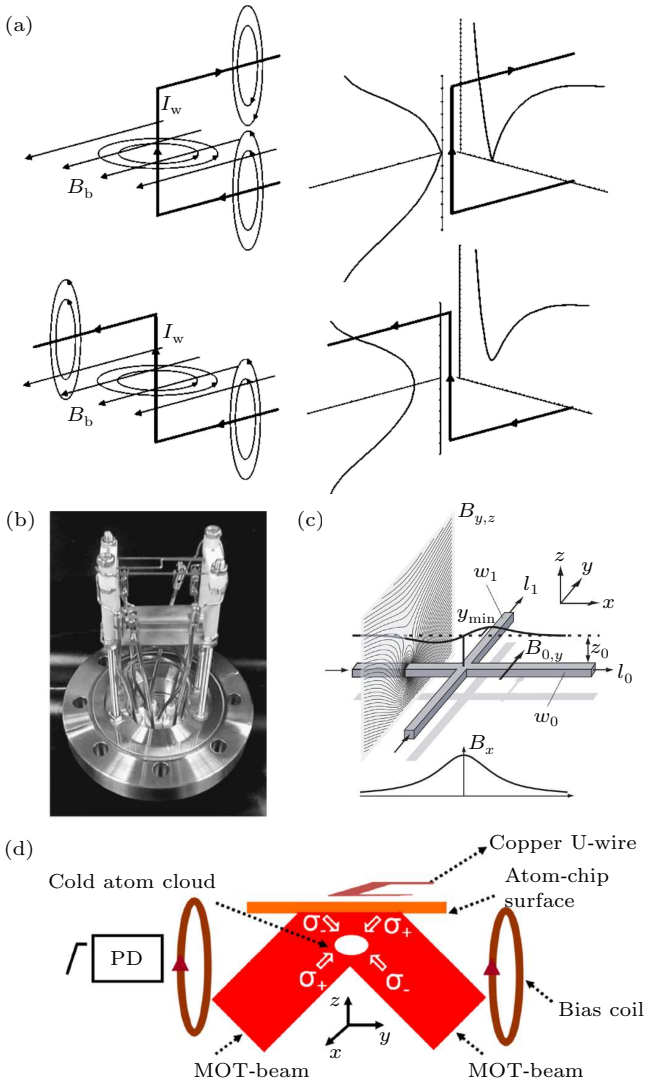


Fig. 2. (a) The magnetic field distributions of U-shaped and Z-shaped wires. The left column shows the geometry, the currents, and the bias magnetic field. The right column shows the radial trapping potential in the horizontal and vertical directions.[192] (b) Picture of the Z-shaped wires.[192] (c) The diagram of cross wire.[193] (d) The diagram of the experimental setup of a U-shaped wire MOT. This scheme uses four laser beams incident on the atom-chip surface to form the optical field. There are two MOT laser beams in the y–z plane, whereas another two MOT laser beams perpendicular to this plane ($\pm x$-direction) are not shown in this diagram.[197]

3. Grating magneto-optical trap

To achieve the compact cold atom systems, researchers have been exploring the miniaturization of MOT systems since

the invention of the first MOT. Apart from the planar magnetic wire system, the optical field has evolved from the conventional six-beam counterpoise laser beams to a single laser beam incident into a conical hollow mirror. During the past few decades, MOT structures based on hollow-cone mirrors have been continuously improved and optimized.[202–206] Despite advancements in miniaturizing MOT, practical applications are still constrained by certain technical and theoretical limitations.

In order to overcome these challenges, a novel manipulation technique has emerged in recent years, namely, the grating MOT (GMOT). In this section, we will describe the principle of GMOT and explore its potential and challenges in practical applications.

There are different ways to simplify light field of the standard MOT. Generally, the two opposing beams in standard MOT are formed by an incident light and its reflection, so only three laser beams are actually needed. To further reduce the laser beams, one laser beam and its reflections by the pyramidal (or conical) hollow mirror can also form the MOT.[207,208] As shown in Fig. 3(a), two sets of reflected light from the four triangular mirrors of the conical hollow structure and one set of light reflected from forward incidence constitute three pairs of cooling lasers perpendicular to each other.[207] This structure can be placed in a vacuum chamber and combined with an anti-Helmholtz coil to realize the cooling and trapping of cold atoms. When a circularly polarized beam of light is incident, the configuration of polarization in a pyramidal (or conical) hollow mirror is also circularly polarized (see Fig. 3(b)).[209] Specially, one may make a small hole in the mirror, so that cold atoms can be led out of the small hole. Such a device is called atomic funnel which could be used to obtain cold atomic beams,[210,211] as shown in Fig. 3(c). Correspondingly, the scheme of a compact cold atomic gravimeter can be realized based on the pyramidal hollow structure with a unique laser beam, leading to a dramatic reduction in system complexity and volume.[212]

In order to facilitate the experiment, the optical path design can be further optimized. Although the use of pyramidal or conical hollow mirror simplifies the design of laser system, it is often necessary to place the mirror inside the vacuum chamber, which complicates the optimization of the optical field. Another approach involves placing the three-mirror trap outside the vacuum chamber.

In 2009, Arnold and co-workers demonstrated that light field in tetrahedral configuration can produce equally effective three-dimensional trapping and cooling, and succeeded in trapping cold atom cloud using the three-reflection-mirror pyramidal hollow structure.[213] The upward beams require an intensity $I_{\rm up} = I_{\rm down}/(3\cos 2\theta)$ for efficient sub-Doppler cooling and balanced optical molasses. Considering a spherical quadrupole magnetic field $\boldsymbol{B} = b(x, y, -2z)$ with symmetry axis along z. The total acceleration formed by the propagation of laser beam is written as

$$\begin{aligned} \boldsymbol{a}_{\rm tot} &= (a_r, a_z) \\ &= 2aC\left[k_\Gamma(\gamma_r v_r, \gamma_z v_z) + \mu_\Gamma b(\kappa_r r, \kappa_z z)\right]\frac{I_{\rm tot}}{I_{\rm sat}}, \end{aligned} \tag{7}$$

where $a = h\pi\Gamma/(m\lambda)$. The detuning of the laser is Δ_Γ in units of Γ, $k_\Gamma = \lambda^{-1}\Gamma^{-1}$ and $C = 8\Delta_\Gamma(1 + I_{\rm tot}/I_S + 4\Delta_\Gamma^2)^{-2}$. The coefficients due to mirror declination can be given as $\gamma_r = \kappa_r = 1/4\sin 2\theta\tan 2\theta$, $\gamma_z = \cos^2\theta$, $\kappa_z = 2\sin^2\theta$. It requires a zero net acceleration $\boldsymbol{a} \propto 0$. Thus, they placed the mirror with the inclination angle of $\theta = 22.5°$, causing the upward beam to converge at an angle 45° above the plane, the schematic is shown in Fig. 3(d). The cooling light field formed by the reflected light from the three mirrors and the incident light simplifies the structure of the system in some measure.

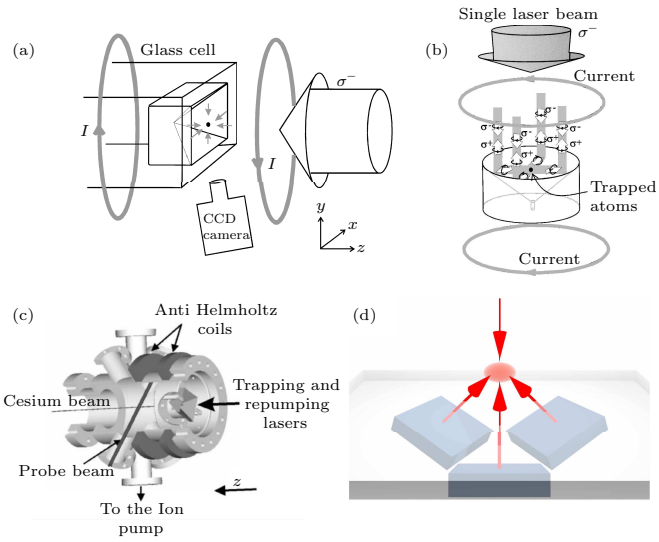


Fig. 3. (a) The experimental setup of pyramidal or conical hollow mirror. The pyramidal or conical hollow mirror is placed inside a glass-cell vacuum chamber. Adapted with permission from Ref. [207] © Optica Publishing Group. (b) The schematics of the experimental setup and the polarization configuration in an axicon-mirror atom trap. Adapted with permission from Ref. [209] © Optica Publishing Group. (c) The sketch of the apparatus for the atomic funnel, the pyramid is formed by two mirrors and two reflecting prisms.[211] (d) The three-dimensional schematic of the demonstration setup using beams reflected from a single downward beam by three mirrors.[213]

However, due to constraints such as the thickness of the vacuum chamber and the height of the working plane of the mirrors, the confined cold atoms are close to the inner wall of the vacuum chamber, posing significant challenges for atom manipulation. Based on the previous research, they proposed an idea to planarize the optical field with three diffraction gratings in 2010.[214] In fact, this is the fundamental work in the planarization of the optical field of the MOT. They utilized three planar diffraction gratings to convert a single laser beam into a four-beam tetrahedral MOT, as illustrated in Fig. 4(a).

The circular region represents the incident area of the single-beam laser, and the arrows depict the propagation directions of diffracted beams in a top view. The grating is positioned beneath the glass vacuum, as shown in the yellow area in Fig. 4(b).

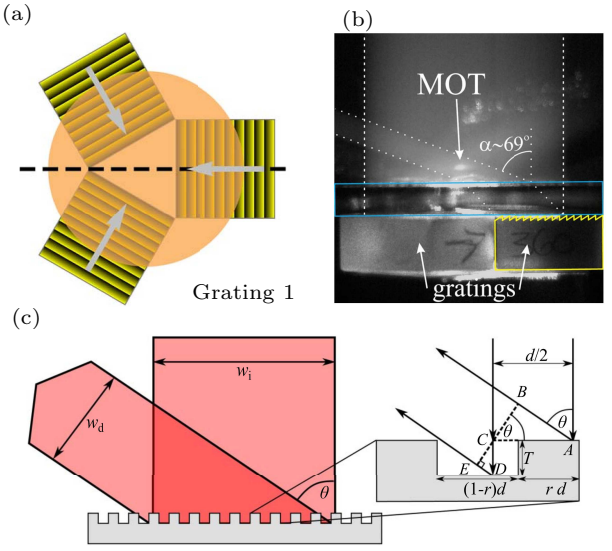


Fig. 4. (a) The top view of three gratings and the circular vertical incident beam. The arrows show the top view of propagation direction of a diffracted beam. Adapted with permission from Ref. [214] © Optica Publishing Group. (b) The side view of the experimental setup. The overlapping region of the downward incident beam (dashed white lines) and the three first-order diffracted beam (dotted white lines) from one grating (yellow line) forms a MOT. The blue line area indicates the 3 mm-thick quartz vacuum chamber, the propagates at the expected $\alpha \sim 69°$. Adapted with permission from Ref. [214] © Optica Publishing Group. (c) The side view of a first-order diffracted beam, illustrating geometric beam compression. Adapted with permission from Ref. [217] © Optica Publishing Group.

The size of the grating is 12.7 mm by 12.7 mm and therefore cannot be fully covered completely by the 23-mm diameter laser. After that, the diffracted beam traverses through a 3 mm-thick quartz vacuum chamber (blue rectangular region in Fig. 4(b)), and the diffraction angle increases to the expected $\alpha \sim 69°$ due to refraction effects (indicated by the dotted white line in Fig. 4(b)). After diffraction, the beams are vertically squeezed to about $w_d = 2.7$ mm, and the atoms are captured in overlapping regions approximating a tetrahedral shape with an overlap volume of about 60 mm^3.

The operational principle of a GMOT is similar to a tetrahedral MOT, and the properties are largely the result of intensity balance and polarization decomposition. The main difference between the tetrahedral MOT and GMOT is that the grating spatially compresses beams with a corresponding intensity increase, as shown in Fig. 4(c). The relationship between incident and reflected intensities of beams is given as

$$I_d/I_i = R_1 w_i/w_d = R_1 \sec\theta, \tag{8}$$

where I_d and I_i respectively represent the intensity of the first-order diffraction and incident beam; the corresponding beam widths are denoted as w_d and w_i. R_1 is the first-order diffraction efficiency, $\theta = \arcsin(\lambda/d)$ is the first-order diffraction angle with wavelength λ and grating period d in the Bragg condition yields.[214] The intensity of the diffraction beam is given as

$$I_{diff} = \eta P_{in}/(A\cos\theta), \tag{9}$$

where η is the diffraction efficiency, P_{in} is the incident light power, and A is the grating area. The total electric field can be represented as

$$\boldsymbol{E}_{tot}/\rho^{1/2} \propto (r + (1-r)d\exp i\phi), \tag{10}$$

$$\phi = \frac{2\pi}{\lambda}(m\lambda/2 - T(1+\cos\theta)), \tag{11}$$

where T is the etch depth, and ρ is the metal reflectivity. Thus, the power ratio of the diffraction and input light is written as

$$\frac{P_m}{P_{in}} = \frac{\rho}{m^2\pi^2}[\sin(m\pi r)^2 + \sin(m\pi S/d)^2 + 2\cos(\phi)\sin(m\pi r)^2\sin(m\pi S/d)], \tag{12}$$

where m represents the diffraction order, $S = (1-r)d - T\tan\theta$ denotes the effective width of the surface. The optical properties of GMOT deserve our attention when designing and optimizing their performance.[215–222] The optical properties of gratings are closely influenced by factors such as coating, period, duty cycle and geometry, where the diffraction efficiency is the key parameter in creating balanced radiation pressure.

From the initial concept proposal to various improvements and optimizations, the GMOT has gone through several stages of development, with technology maturing and application areas expanding. Based on the three-GMOT, various different types of GMOTs have been proposed. In 2013, Arnold's group improved the three-GMOT using reactive ion etching, where the grating was etched to a depth of $\lambda/4$ with a period of 1200 nm. Subsequently, they sputter-coated the grating with 200 nm of gold, followed by a 10 nm chromium layer to achieve a reflectivity of ~ 0.97. The efficiency of the first-order diffracted light reached 40(1)%, with the trapped atom number reached 6.4×10^6. Furthermore, they integrated three diffractive gratings onto a single silicon-based grating chip, realizing integrated three linear GMOT, as illustrated in Fig. 5(a). Integrated three linear GMOT was deposited with a 3 nm layer of nickel-chromium and a 10 nm layer of aluminum for reflection, with a first order diffractivity of 38(1)% and a grating period of 1400 nm. Owing to the additional diffracted beam loss induced by the quartz vacuum glass cavity surface, integrated three linear GMOT is close to the ideal diffractivity $\sim 1/3$ required for the balance radiation pressure in an optical molasses, yielding a sub-Doppler temperature of 50 μK–60 μK. In addition, they constructed square grating and circular grating, as shown in Figs. 5(b) and 5(c), both made of

silicon or gallium arsenide, with a 3 nm nickel-branded adhesive layer and a 100 nm gold reflective coating. With a period of 1080 nm, 20(1)% of the incident power was diffracted into four first-order beams.[223] Another proposed scheme involved the use of a ring-shaped concave grating reflector to confine atoms optically, as shown in Fig. 5(d).[224] The ring grating has a strong focusing capability at radial polarization, providing deep potentials to trap cold atoms. Recently, the Zou's research group achieved a breakthrough in planarizing the magnetic field coils,[225] realizing an integrated MOT system based on dual chips (grating chip and coil chip), as depicted in Fig. 5(e). The coil chip was placed alongside the grating chip outside the vacuum chamber. By perpendicular incidence of a beam containing cooling and repumping light onto the grating chip, and in combination with a quadrupolar magnetic field generated by the magnetic field chip below, the cloud of cold atoms is trapped within the vacuum cavity at a location above the chip. The temperature of the atomic cloud can be measured by absorption imaging and time-of-flight method (see Fig. 5(f)), extracting the axial temperature of 382 μK and a radial temperature of 1.37 mK for the atom cloud.

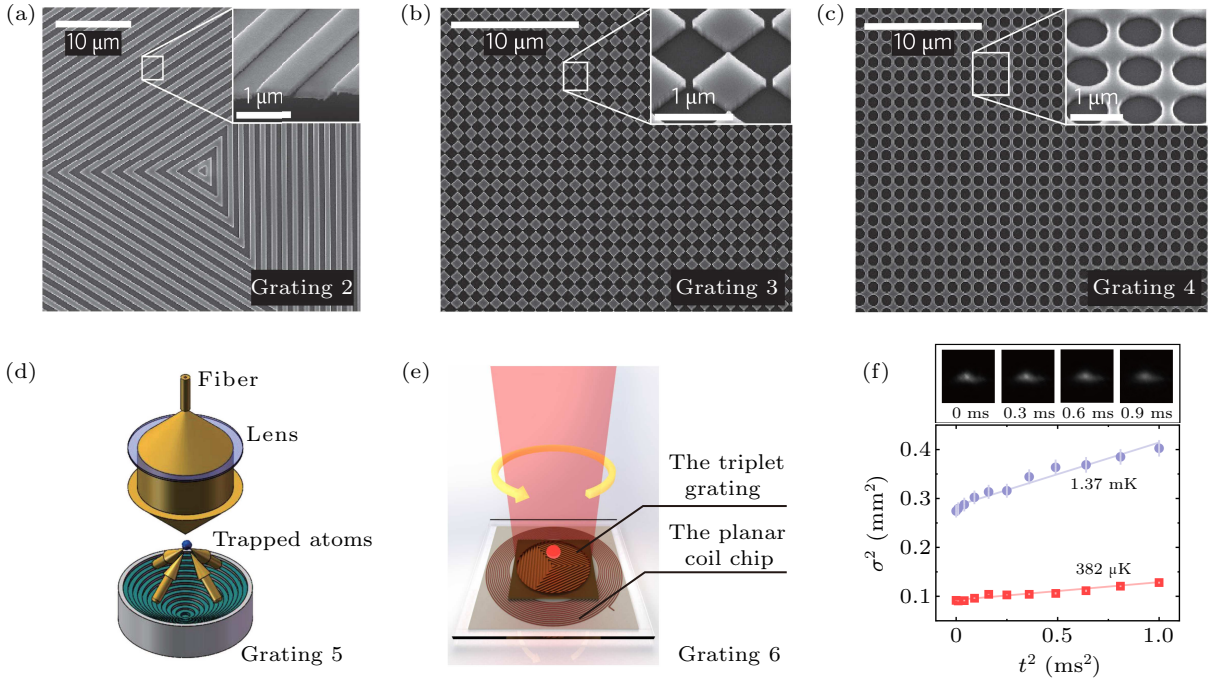


Fig. 5. (a) The integrated three linear grating extends the pattern of the three gratings inward to the center and outward over a 20 mm × 20 mm area, which has a pitch of $d = 1400$ nm ($\alpha = 34°$). The inset shows the scanning electron microscope close-up of the etched area. (b) The squares covering a total area of 2 cm × 2 cm, with a pitch of $d = 1080$ nm ($\alpha = 46°$). The inset shows the zoomed image. (c) The circular grating is the same as the square grating, but with squares replaced by circles.[223] (d) The schematic of the ring grating optical focusing trapping under radially polarized illumination. The radially polarized light diverges from the optical fiber and passes through a focal lens then illuminates the ring grating.[224] (e) The schematic of the planar-integrated MOT. The left-hand incident laser beam propagates perpendicular to the integrated three linear grating and traps a cold atom cloud in the presence of the coil chip.[225] (f) The experimental performance of the planar-integrated MOT. The top figure shows the absorption images of cold atomic cloud after free expansion, and the bottle shows axial (red point) and radial (purple point) radius fitting curves for atomic clouds.[225]

In Table 1, the performance indexes of various types of GMOTs, including the number of trapped atoms and the temperature of the atomic cloud, are listed in detail. These performance indexes reveal the advantages and disadvantages of different types of GMOTs. Some GMOTs perform well at trapping atoms (such as grating 4), effectively trapping large numbers of atoms, while others perform at lowering the temperature of the atomic cloud (grating 1), allowing for even lower atomic temperatures. In addition, there are GMOTs that offer advantages such as fast processing (grating 5) and a high degree of integration (grating 6, also see the chip-scale packages for laser cooling platform in Refs. [226–228]). How to integrate these performance advantages into a single grating chip is an area worthy of further exploration and innovation. This improved integration capability will greatly boost the development of GMOT technology and provide broader prospects for its application in different fields.

Table 1. Capability of different types of GMOTs for neutral atoms.

Type	Atomic number	Temperature
Three linear gratings[214]	6.4×10^6	30 ± 10 μK
Integrated three linear grating[223]	1.7×10^7	50–60 μK
Square grating[223]	5.3×10^7	–
Circular grating[223]	5.9×10^7	–
Ring grating[224]	–	1.14 mK
Integrated three linear grating[225]	2.3×10^6	382 μK

The atoms trapped by the gratings are ^{87}Rb.

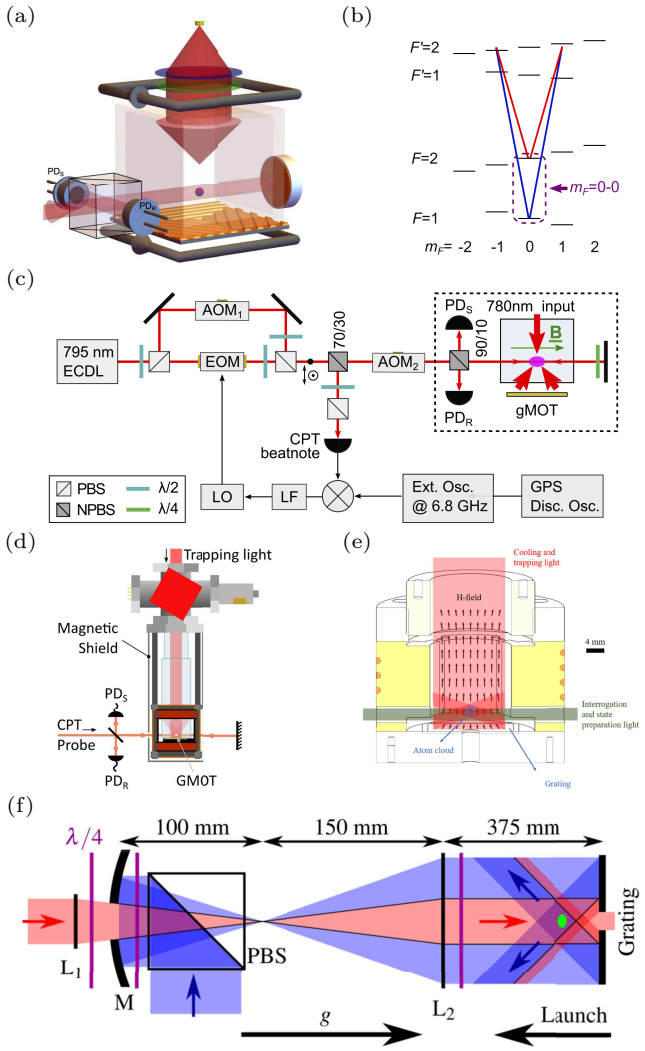


Fig. 6. (a) The schematic diagram of CPT detection based on GMOT. (b) The schematic diagram for lin ⊥ lin CPT on the D_1 line of ^{87}Rb. (c) The schematic diagram of optical bench for the CPT experimental. The dashed region indicates the GMOT and CPT signal zone.[230] (d) The top-down view of the clock apparatus. The atoms within a Rb GMOT are probed using CPT in a lin ⊥ lin polarization scheme.[231] (e) The concept of a microwave cavity with integrated grating. The ensemble is placed in a vacuum chamber.[232] (f) The optics for a grating-chip launch with the gravity in the g direction. The inner beam (red path) hits the atoms only from above, while the outer beam (blue path) hits the atoms only from below.[233]

Cold atoms allow for ultra-low-drift metrology with excellent precision in physical observations.[229] Recently, it has been proposed to utilize the compact optical layout of a GMOT to obtain an accurate frequency reference.[230] Collecting 10^7 ^{87}Rb atoms subsequently cooled to 20 μK in optical molasses, the GMOT is used to develop the coherent population trapping (CPT) clock by pulsed Ramsey probing (see Fig. 6(a)). The clock signal is measured by the two photodiodes (PD_{RS} for reference/signal). The diagrams of energy levels and optical layout of the CPT are shown in Figs. 6(b) and 6(c), respectively. By using this scheme, the short-term fractional frequency stability of compact cold-atom CPT clock is $2\times10^{-11}/\sqrt{\tau}$, and prospects for $2\times10^{-13}/\sqrt{\tau}$ at the quantum projection noise limit. A year later, they also reported the recent progress in the research of cold atom microwave clocks in small packages.[231] The experimental setup is shown in Fig. 6(d), the short-term stability was measured to be $5\times10^{-11}/\sqrt{\tau}$. Moreover, it has been proposed an additive-manufactured microwave cavity utilizing the compact atomic clock based on the GMOT,[232] with its schematic diagram shown in Fig. 6(e). Except for cold atomic clocks mentioned above, the GMOT also has applications in cold atomic fountain.[233] Cold atomic fountain clocks offer exceptional long-term stability at the expense of a larger size. Figure 6(f) illustrates the optics of the grating chip launch at a gravity of g direction. The internal beam (red path) can only hit atoms from above, while the external beam (blue path) can only hit atoms from below. The experimental results showed the Ramsey time up to 100 ms with a corresponding fringe linewidth of 5 Hz, and the best single-shot fractional stability of 3.1×10^{-11} was measured. This technology improves the short- and long-term stability of atomic clocks while maintaining compactness for portable applications.

In addition to applications in atomic clocks, GMOT plays an important role in other quantum sensors. A schematic of the extremely miniaturized cold atom interferometer accelerometer is shown in Fig. 7(a).[234] It depicts in detail the cooled beam for the GMOT and the configuration of the atom detection channel. In this compact sensor head containing a vacuum package, sub-Doppler cooling of the GMOT achieves 15 μK temperature and the the GMOT can operate at a data rate of 20 Hz. They demonstrated the measured gravity $g = 9.79316(2)$ ms^{-2} with the light-pulse atom interferometer operation up to $T = 4.5$ ms, and the statistical uncertainty was $\Delta g/g = 2.0\times10^{-6}$. Other studies have proposed compact systems of single-beam laser Zeeman slower and MOTs created by nanofabricated diffraction gratings.[235] The schematic of the experimental setup is shown in Fig. 7(b), the hole in the grating allows atoms to be loaded into the system from a heated atomic dispenser while increasing the interaction distance between the atoms and the laser, improving the atom trapping efficiency. The lowest Zeeman coil effectively decelerates the initial velocity of the atoms, which in turn is captured by the GMOT. This compact GMOT and Zeeman reducer design is suitable for a wide range of atomic and molecular cooling, and has potential applications for the development of quantum technologies based on cold atoms.

Moreover, there are studies proposing compact ultracold electron sources based on GMOTs.[236] The schematic diagram of the experiment is shown in Fig. 7(c), this ultrafast and ultracold electron source utilizes near-threshold photoionization of trapped clod atomic gas, providing a unique combination of low transverse beam emittance and high beam bunch charge. This ultracold electron source based on the GMOT offers the possibility of realizing picosecond electron pulses with

high beam bunch charges. In addition, the study in Fig. 7(d) successfully integrated a GMOT in a 4 mm thick Si/glass vacuum cell.[237] To overcome the limitations in GMOT imaging due to surface scattering, the researchers used a two-step optical excitation process of rubidium atoms with 420 nm fluorescence detection. This miniaturized laser cooling platform provides an enabling platform for the development of compact cold atom quantum sensors.

As a compact, efficient and versatile atom cooling and trapping technology, GMOTs enable the trapping and control of atoms with a single laser beam, greatly simplifying system design and operating procedures. The high efficiency of capture and loading rates, flexibility for a wide range of atomic and molecular species, compatibility with miniaturization techniques, and high data-rate operation and temperature control make it an important tool for future applications in cold atom technology and quantum technology, opening up new possibilities in the development of compact atomic sensors and instrumentation.

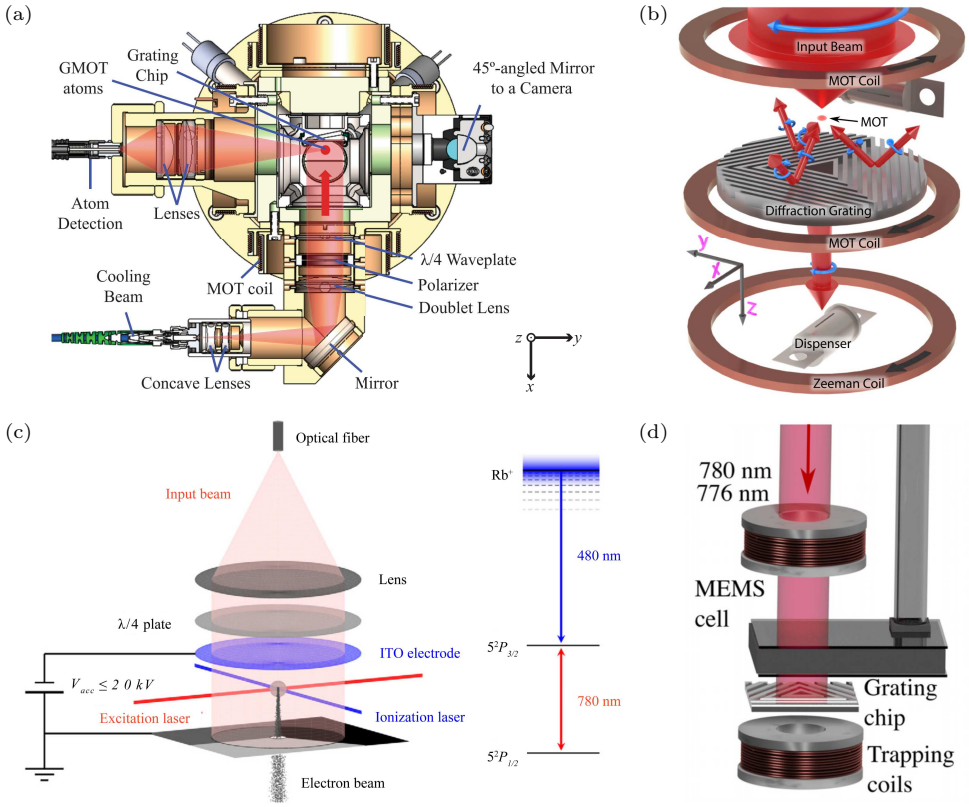


Fig. 7. (a) The horizontal cross-sectional renderings of the compact light-plus atom interferometer sensor head. The cooling-channel light with a large collimated Gaussian beam is delivered to the sensor head via a polarization maintaining fiber. The GMOT atoms (solid red circle) form ~ 3.5 mm from the grating surface.[234] (b) The illustration of the Zemman slower and integrated three linear GMOT experimental apparatus. The lithium atoms that leave the heated dispenser are slowed by the Zeeman coil and then captured by the GMOT.[235] (c) The schematic representation of the ultracold electron source based on a GMOT. The electrons are accelerated and pass through the center hole of the earth-grounded grating.[236] (d) The micro-electro-mechanical-systems cell based on GMOT illustration, which provides a promising platform for future compact cold-atom sensors.[237]

4. Metasurface magneto-optical trap

In the development of GMOT technology, there are new technologies emerging. For promoting the further development of cold atom technology, as a new technique, metasurface MOT has emerged in recent decade. The metasurface is a planar material consisting of artificial structures at subwavelength scales that precisely control the propagation properties of light, including polarization, phase, and amplitude. With the precision-designed surface structure, the metasurface MOT is a potential means of solving these problems such as asymmetry of the captured atomic region and low utilization of optical energy in GMOT. In this section, we will present the principles of metasurface MOT and its development. It will help us have a better understanding of the potential of this emerging technology and build a robust foundation for future research and applications.

With the continuous advancement of micro and nanofabrication technologies,[238] optical devices are progressing towards miniaturization, integration and light weight. This trend not only significantly reduces the space required for optical path systems but also greatly expands their potential applications in commercial equipment. Metasurface has attracted considerable attention due to its compact size, high degree of integration, and flexible performance design. It is an ar-

tificial microstructure device composed of nanostructure arrays with subwavelength scale. Through special design of its own micro-nanostructure in terms of geometric shape and materials, metasurface can precisely manipulate optical waves. Compared to the traditional optical component, metasurface exhibits greater operating bandwidth, more compact structure, and higher integration.

Traditional optical devices typically rely on the accumulation of phase as light propagates through different media, with refraction and reflection phenomena that can be described by Snell's law. However, optical devices designed based on this approach are generally thicker, which is not suitable for the trend of miniaturization and integration.

In contrast, metasurface introduces an abrupt phase shift at the wavelength scale, adding a new degree of freedom to optical system. This characteristic of abrupt phase shift enables metasurface to achieve complex light field manipulation within extremely small dimensions. In 2011, Capasso from Harvard University led his team to propose the idea of designing resonant phase metasurface.[239] They constructed nanoantennas with different equivalent refractive indices and proposed generalized laws of reflection and refraction, which are written as

$$\begin{cases} n_{\mathrm{t}}\sin(\theta_{\mathrm{t}}) - n_{\mathrm{i}}\sin(\theta_{\mathrm{i}}) = \dfrac{\lambda_0}{2\pi}\dfrac{\mathrm{d}\varphi}{\mathrm{d}x}, \\ \sin(\theta_{\mathrm{r}}) - \sin(\theta_{\mathrm{i}}) = \dfrac{\lambda_0}{2\pi n_{\mathrm{i}}}\dfrac{\mathrm{d}\varphi}{\mathrm{d}x}, \end{cases} \tag{13}$$

where n_{t}, n_{i} are the refractive indices of the two media; θ_{t}, θ_{i}, and θ_{r} are the refraction, incident and reflection angles, respectively; λ_0 is the vacuum wavelength. The design of subwavelength resonance units in the metasurface allows the artificial control of this introduced phase shift φ. When $\mathrm{d}\varphi/\mathrm{d}x = 0$, the above law degenerates into the classic Snell's law. The schematic diagram of Snell and generalized Snell's law on a metasurface is shown in Fig. 8(a). Therefore, one can achieve refraction or reflection in any direction of beam simply by introducing an appropriate phase gradient change at the interface. Based on this principle, they proposed a method of controlling the opening direction of a V-shaped structure in order to achieve precise control of the phase of reflected light from 0 to 2π, as shown in Fig. 8(b). The unit cell of plasmonic interface (yellow) comprises eight gold V-antennas of ~ 220 nm and ~ 50 nm, and it repeats with a periodicity of 11 μm in the x-direction and 1.5 μm in the y-direction. The scattered electric field of V-antennas unit cell polarized in the x-direction for y-polarized plane wave excitation is shown in Fig. 8(c).

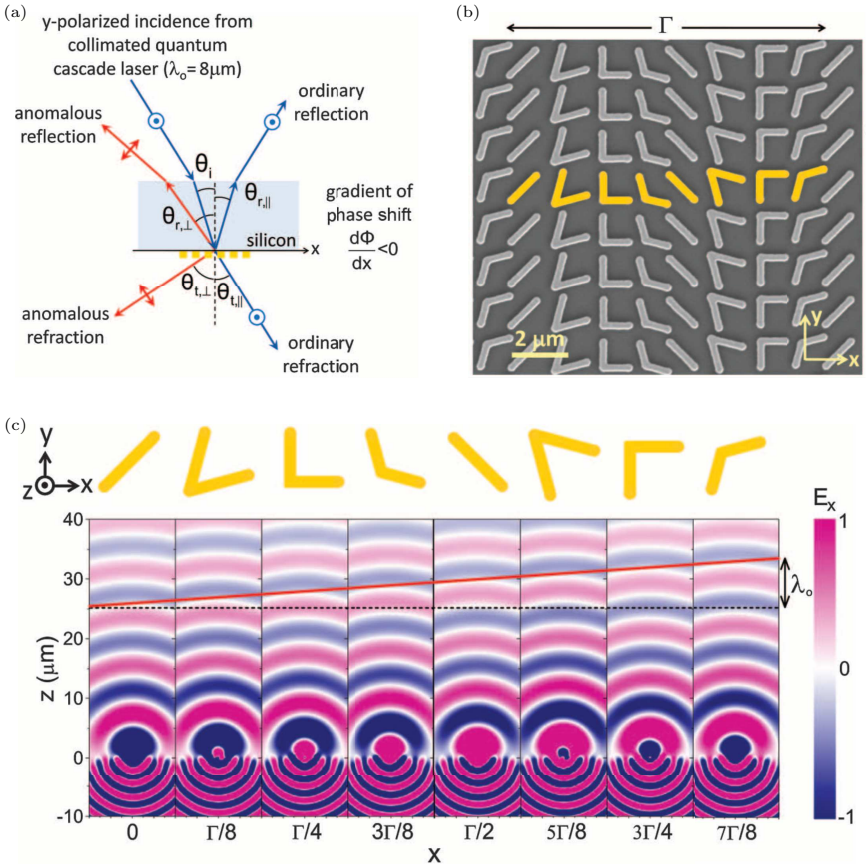


Fig. 8. (a) The schematic diagram of Snell's and generalized Snell's law for y-polarized excitation with the electric field normal to the plane of incidence. (b) The scanning electron microscope image of resonant phase metasurface on a silicon wafer. (c) The scattered electric field for the individual antennas composing the array.[239]

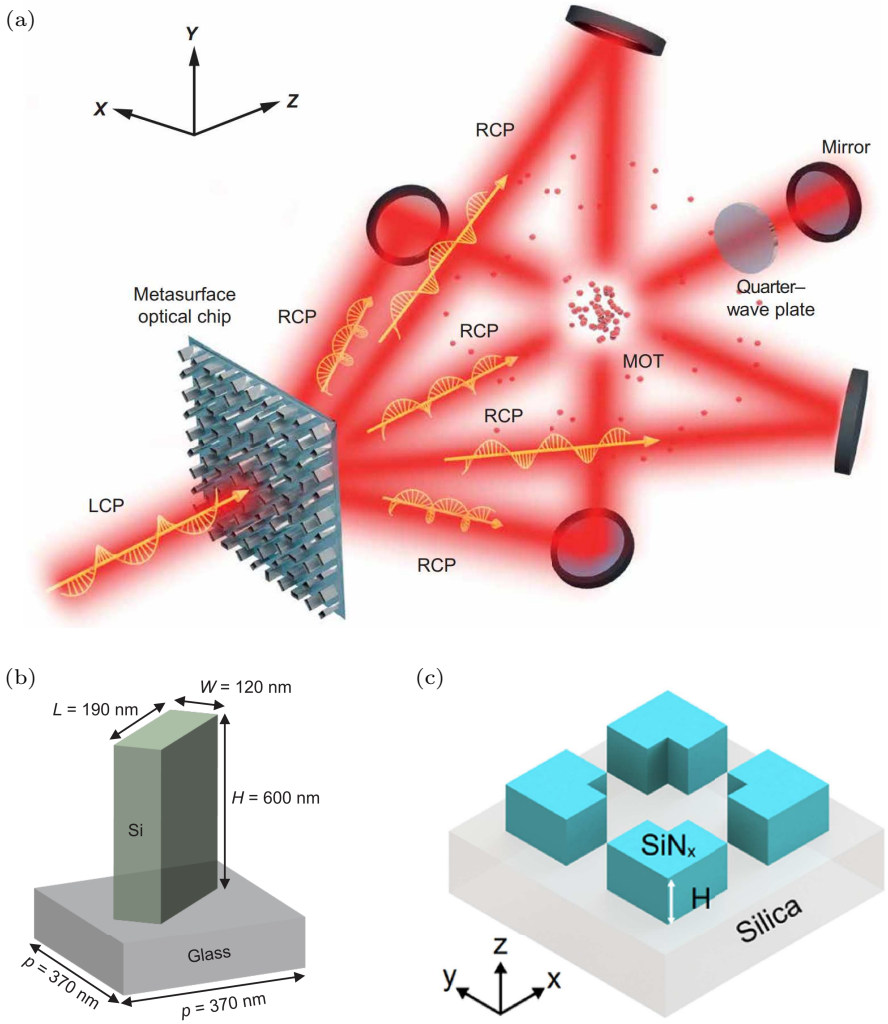


Fig. 9. (a) The metasurface has been engineered to diffract an incident laser beam into five distinct beams, each with predefined directions and circular polarization states. (b) The geometric configuration of the meta-atom.[240] (c) The geometrical configuration of the metasurface with height $H = 392$ nm.[241]

This subwavelength antenna can be considered as an optical resonator. The incident light induces displacement currents in the resonator when its wavelength is close to the resonant wavelength of the structure, resulting in a significant change in the phase relationship between the scattered and incident fields. This change further causes a strong scattering of electromagnetic fields into free space, which is called the resonance phase in metasurfaces. In addition to this, the physical mechanisms of metasurfaces include geometry phase and propagation phase. The geometric phase comes from the change in the polarization state of the light wave as it passes through the microstructure, and the propagation phase is the accumulated phase change due to the propagation of the light through the medium. These mechanisms enable efficient manipulation of light at subwavelength scales on metasurfaces.

With the continuous development of metasurface technology, researches have introduced it into the study of MOT. With appropriate phase gradient shifts introduced on the metasurface, precise control and trapping of atoms can be achieved. Specifically, the working principle of the metasurface MOT includes the following steps. First of all, the appropriate subwavelength resonant structures are designed on the metasurface, which can be prepared by micro- and nanofabrication techniques. Subsequently, by adjusting parameters such as the geometry, spacing and material properties of the resonant units, the response of the metasurface to light can be adjusted to achieve specific phase modulation. Once this phase gradient shift is introduced on the metasurface, it is possible to produce localized phase variations in space, thus enabling precise control of the beams. The emergence of metasurface MOT represents a further development in the field of cold atom physics.

In 2020, the team led by Li from China proposed a metasurface optical chip for generating ensembles of cold atoms,[240] providing a new approach for realizing a single-beam MOT, as illustrated in Fig. 9(a). The design of the metasurface diffracts a single beam of left circular polarization of incident light into five beams with predetermined directions, which possess the same intensity and circular polarizations. One of these beams propagates along the incident direction, while the remaining four beams are deflected by 22.5° rela-

tive to the incident beam along the $\pm x$ and $\pm y$ axes. With five mirrors, all beams intersect at the center of a quadrupole magnetic field, realizing three-dimensional cooling and trapping. In the process of designing the metasurface, they use a reciprocal process to superimpose five output beams together at the metasurface plane ($z = 0$ plane). Thus, the Pancharatnam–Berry phase type metasurface phase profile is given by

$$\Phi(x,y) = \arg\left(\sum_{n=0}^{4} A_n \cdot \mathrm{e}^{-\mathrm{i}\cdot \boldsymbol{k}_n \cdot \boldsymbol{r}_n}\right), \tag{14}$$

where the arg function is the argument of the complex amplitude; $n = 0,1,2,3,4$ indicate the five output beams and A_n are the electric field amplitudes of the five beams. The geometrical configuration of the meta-atom of the metasurface with period $p = 370$ nm is shown in Fig. 9(b), the length, width and height of meta-atom are $L = 190$ nm, $W = 120$ nm and $H = 600$ nm, respectively. Such a metasurface MOT can trap up to $\sim 10^7$ atoms and the temperature of atoms reaches 35 μK. Based on this study, they proposed another metasurface MOT with a schematic meta-atomic structure shown in Fig. 9(c).[241] The improved metasurface MOT is capable of trapping up to $\sim 1.4 \times 10^8$ atoms and its temperature reaches ~ 7.0 μK, which is a significant improvement in performance.

More recently, it has also been proposed to utilize a combination of metasurface and grating to trap cold atoms,[242] which is schematically shown in Fig. 10(a). The photonic integrated circuit launches a linear polarization Gaussian beam, which is subsequently shaped by the metasurface, the unit cell of metasurface is shown in Fig. 10(b). The performance of this planar optical MOT is comparable to that of a Gaussian beam GMOT. In addition, the integrated optical structure that enables compact strontium atomic clocks to be realized on metasurface has been proposed, which is schematically shown in Fig. 10(c).[243] It includes a pair of 0° (light color) and 45° (dark color) red and blue beams, and a colinear combination of lattice and clock beams (yellow). The alignment diagram of photonic integrated circuit and metasurface in the bottom is shown in Fig. 10(d). The inset shows the bonded device (top) and a scanning electron microscopy (SEM) image of metasurface (bottom). This integrated design provides a scalable approach to realizing complex optical systems that may be integrated with a vacuum chamber for physics experiments in the future, which provides a unique technology platform for atomic clocks.

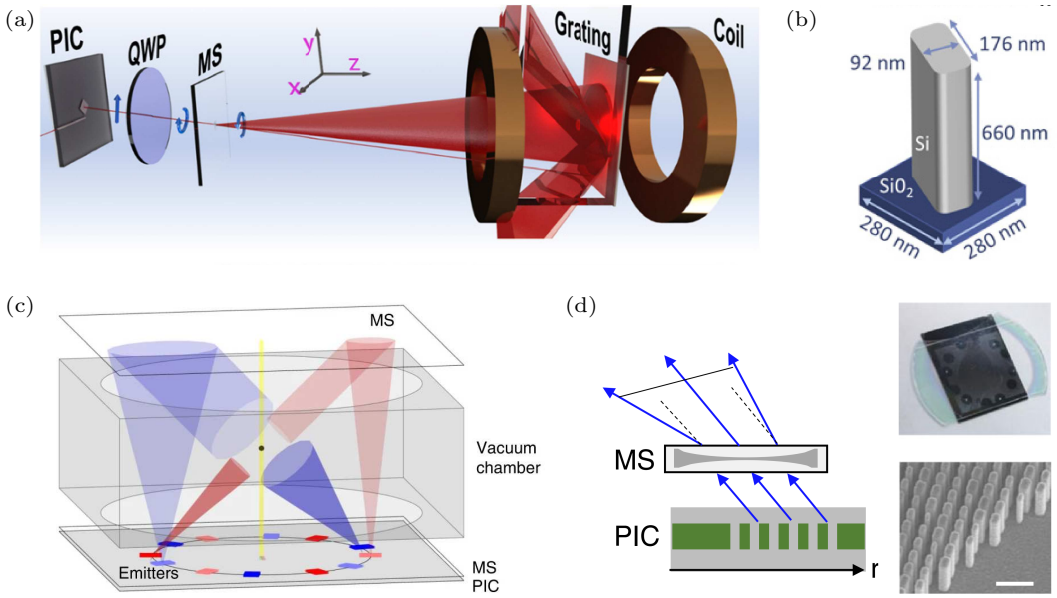


Fig. 10. (a) The planar optics GMOT with metasurface. The metasurface produces an expanding mode featuring opposite polarization (depicted as a red cone), thereby achieving a flat-top intensity profile at the integrated three linear gratings. (b) The schematic of metasurface unit cell with quarter-wave phase pillar.[242] (c) The photonics geometry as a party of the strontium clock. (d) The diagram of photonic integrated circuits and metasurface alignment. The insets show the picture of the bonded device (top) and SEM of nanopillars.[243]

5. Summary and outlook

In this review, we introduce the compact MOTs using planar optics. The advantage of a standard MOT is that it provides an isotropic trapping force, allowing for uniform control of particles in space. The MOT with planar wire simplifies the structure of current coils. We introduce two compact MOTs based on planar optics: the grating-based MOTs (GMOTs) and the metasurface-based MOTs. The grating creates a specific distribution of light field, which combines with the magnetic field to create a capturing force. The GMOTs have greatly simplified the incident beams in traditional MOTs, which are characterized by small size, abundant optical windows and high scalability. It has been widely used to build cold atomic clocks, interferometers, ultra-cold electron sources.[244,245] The meta-

surface MOTs are a novel type of MOTs using nanofabrication technology. The metasurface is a surface structure with special optical properties that allows precise control of the optical field by adjusting the shape and material of the surface. These new MOT techniques overcome the limitations of traditional techniques, reduce volume and power consumption, and expand the application prospects of MOTs.

In recent decades, chip-scale MOTs offer advantages such as smaller size and low-power dissipation, providing more convenient conditions for practical applications.[162,226,227,237] Especially, ultra-high-vacuum environments can be kept for six months without active pumping using micro-electromechanical-systems (MEMS) alkali vapor cells,[237,246] which largely reduces the volume burden of the MOT vacuum system. The combination of chip-scale device with MEMS can further reduce the size of the MOT. In addition, the manipulation of atom chips in chip-scale MOT gradually evolved from the initial single magnetic trap structure to multifunctional devices.[247]

Additionally, miniaturized optical systems can be constructed using planar optics. Photonic integrated circuit (PIC) offers a rich set of passive and active components with low optical losses, and presents new opportunities for the development of MOT.[164,234,242,243] And the metasurface can produce beams with a high numerical aperture (NA), arbitrary tilt angle, prescribed polarizations, and collinear propagation.[243,248] The combination of the manufacturability of PICs and the multifunctionality of metasurface enables the construction of complex optical systems with multiple beam emitters on chips.

Acknowledgments

Project supported by the National Key Research and Development Program of China (Grant No. 2022YFA1404104), the National Natural Science Foundation of China (Grant Nos. 12025509 and 12104521), and Fundamental Research Project of Shenzhen (Grant No. JCYJ20230808105009018).

References

[1] Wineland D J and Itano W M 1979 *Phys. Rev. A* **20** 1521
[2] Steane A M, Chowdhury M and Foot C J 1992 *J. Opt. Soc. Am. B* **9** 2142
[3] Kowalski K, Long V C, Xuan K D, Głódź M, Huy B N and Szonert J 2010 *CMST* **SI(2)** 115
[4] Liu Y, Wu J H, Shi B S and Guo G C 2012 *Chin. Phys. Lett.* **29** 024205
[5] Shimizu F, Shimizu K and Takuma H 1991 *Opt. Lett.* **16** 339
[6] Marcassa L, Bagnato V, Wang Y, Tsao C, Weiner J, Dulieu O, Band Y B and Julienne P S 1993 *Phys. Rev. A* **47** R4563
[7] Drewsen M, Laurent Ph, Nadir A, Santarelli G, Clairon A, Castin Y, Grison D and Salomon C 1994 *Appl. Phys. B* **59** 283
[8] Chesman C, Lima E G, de Oliveira F A M, Vianna S S and Tabosa J W R 1994 *Opt. Lett.* **19** 1237
[9] Anderson M H, Ensher J R, Matthews M R, Wieman C E and Cornell E A 1995 *Science* **269** 198
[10] Schadwinkel H, Reiter U, Gomer V and Meschede D 1999 *Phys. Rev. A* **61** 013409
[11] Han J X, Lu B Q, Yin M J, Wang Y B, Xu Q F, Lu X T and Chang H 2019 *Chin. Phys. B* **28** 013701
[12] Zhang D, Li Y Q, Wang Y F, Fu Y M, Li P, Liu W L, Wu J Z, Ma J, Xiao L T and Jia S T 2020 *Chin. Phys. B* **29** 023203
[13] Stuhl B K, Sawyer B C, Wang D and Ye J 2008 *Phys. Rev. Lett.* **101** 243002
[14] Chang X F, Ji Z H, Yuan J P, Zhao Y T, Yang Y G, Xiao L T and Jia S T 2013 *Chin. Phys. B* **22** 093701
[15] Barry J F, McCarron D J, Norrgard E B, Steinecker M H and DeMille D 2014 *Nature* **512** 286
[16] Tarbutt M R 2015 *New J. Phys.* **17** 015007
[17] McCarron D J, Norrgard E B, Steinecker M H and DeMille D 2015 *New J. Phys.* **17** 035014
[18] Tarbutt M R and Steimle T C 2015 *Phys. Rev. A* **92** 053401
[19] Xie D, Bu W and Yan B 2016 *Chin. Phys. B* **25** 053701
[20] He J, Liu B, Wang J Y, Diao W T, Jin G and Wang J M 2017 *Chin. Phys. B* **26** 113702
[21] Xu S, Xia M, Gu R, Yin Y, Xu L, Xia Y and Yin J 2019 *Phys. Rev. A* **99** 033408
[22] Baum L, Vilas N B, Hallas C, Augenbraun B L, Raval S, Mitra D and Doyle J M 2020 *Phys. Rev. Lett.* **124** 133201
[23] Jurgilas S, Chakraborty A, Rich C J H, Sauer B E, Frye M D, Hutson J M and Tarbutt M R 2021 *New J. Phys.* **23** 075004
[24] Lin Z, Shimizu K, Zhan M, Shimizu F and Hiroshi Takuma H T 1991 *Jpn. J. Appl. Phys.* **30** L1324
[25] Li K, Zhang D, Gao T, Peng S G and Jiang K 2015 *Phys. Rev. A* **92** 013419
[26] Chen Y D, Li W X, Chou M E, Kuo C H, Li C S and Tung S 2021 *Phys. Rev. A* **103** 023102
[27] Raab E L, Prentiss M, Cable A, Chu S and Pritchard D E 1987 *Phys. Rev. Lett.* **59** 2631
[28] Zhang F, Long Y, Yang J L, Ma G Q, Yin J P and Wang R Q 2015 *Chin. Phys. Lett.* **32** 123701
[29] Zhang X X, Zheng H Q, Ge L L, Zhao H, Ren Q Y and Ma X Q 2020 *Opt. Commun.* **470** 125793
[30] Liu W, Zheng N, Wang X, Xu J, Li Y, Sovkov V B, Li P, Fu Y, Wu J, Ma J, Xiao L and Jia S 2021 *J. Phys. B: At. Mol. Opt. Phys.* **54** 155501
[31] Williamson R S and Walker T 1995 *J. Opt. Soc. Am. B* **12** 1393
[32] Goldwin J, Papp S B, DeMarco B and Jin D S 2002 *Phys. Rev. A* **65** 021402
[33] Wei D, Xiong D, Chen H, Wang P, Guo L and Zhang J 2007 *Chin. Phys. Lett.* **24** 1541
[34] Zeng Z, Li S and Yan B 2021 *Front. Phys.* **17** 32502
[35] Wallace C D, Dinneen T P, Tan K Y N, Grove T T and Gould P L 1992 *Phys. Rev. Lett.* **69** 897
[36] Fox R W, Robinson H G, Gilbert S L, Hollberg L and Marquardt J H 1993 *Opt. Lett.* **18** 1456
[37] Xu B M, Chen X, Wang J and Zhan M S 2008 *Opt. Commun.* **281** 5819
[38] Zhang S, Chen J F, Liu C, Zhou S, Loy M M T, Wong G K L and Du S 2012 *Rev. Sci. Instrum.* **83** 073102
[39] Xiang J F, Cheng H N, Peng X K, Wang X W, Ren W, Ji J W, Liu K K, Zhao J B, Li L, Qu Q Z, Li T, Wang B, Ye M F, Zhao X, Yao Y Y, Lü D S and Liu L 2018 *Chin. Phys. B* **27** 073701
[40] Zhu C J, Guan J, Zhou F, Zhu E Y and Li Y 2021 *OSA Continuum* **4** 2527
[41] Monroe C, Swann W, Robinson H and Wieman C 1990 *Phys. Rev. Lett.* **65** 1571
[42] Telles G D, Garcia W, Marcassa L G, Bagnato V S, Ciampini D, Fazzi M, Müller J H, Wilkowski D and Arimondo E 2001 *Phys. Rev. A* **63** 033406
[43] Xu X, Loftus T H, Smith M J, Hall J L, Gallagher A and Ye J 2002 *Phys. Rev. A* **66** 011401
[44] Yan S B, Geng T, Zhang T C and Wang J M 2006 *Chin. Phys.* **15** 1746
[45] Ma J, Wang L R, Ji W B, Xiao L T and Jia S T 2007 *Chin. Phys. Lett.* **24** 1904
[46] Zhang P, Li G, Zhang Y C, Guo Y, Wang J and Zhang T 2009 *Phys. Rev. A* **80** 053420
[47] Feng Z, Zhang H, Che J, Zhang L, Li C, Zhao J and Jia S 2011 *Phys. Rev. A* **83** 042711
[48] Li Y, Wu J, Feng G, Nute J, Piano S, Hackermüller L, Ma J, Xiao L and Jia S 2015 *Laser Phys. Lett.* **12** 055501
[49] Pei D L, He J, Wang J Y, Wang J C and Wang J M 2017 *Acta Phys. Sin.* **66** 193701 (in Chinese)

[50] Simsarian J E, Ghosh A, Gwinner G, Orozco L A, Sprouse G D and Voytas P A 1996 *Phys. Rev. Lett.* **76** 3522
[51] Lu Z T, Corwin K L, Vogel K R, Wieman C E, Dinneen T P, Maddi J and Gould H 1997 *Phys. Rev. Lett.* **79** 994
[52] Sengstock K and Sterr U M 1994 *Appl. Phys. B* **59** 99
[53] Goncharov A N, Bonert A E, Brazhnikov D V, Shilov A M and Bagayev S N 2014 *Quantum Electron.* **44** 521
[54] Prudnikov O N, Brazhnikov D V, Taichenachev A V, Yudin V I and Goncharov A N 2016 *Quantum Electron.* **46** 661
[55] Kurosu T and Shimizu F 1990 *Jpn. J. Appl. Phys.* **29** L2127
[56] Mills M, Puri P, Yu Y, Derevianko A, Schneider C and Hudson E R 2017 *Phys. Rev. A* **96** 033402
[57] Katori H, Ido T, Isoya Y and Kuwata-Gonokami M 1999 *Phys. Rev. Lett.* **82** 1116
[58] Maruyama R, Wynar R H, Romalis M V, Andalkar A, Swallows M D, Pearson C E and Fortson E N 2003 *Phys. Rev. A* **68** 011403
[59] Zhao P Y, Xiong Z X, Liang J, He L X and Lu B L 2008 *Chin. Phys. Lett.* **25** 3631
[60] Xu X Y, Wang W L, Zhou Q H, Li G H, Jiang H L, Chen L F, Ye J, Zhou Z H, Cai Y, Tang H Y and Zhou M 2009 *Front. Phys. China* **4** 160
[61] Zhou M, Chen N, Zhang X H, Huang L Y, Yao M F, Tian J, Gao Q, Jiang H L, Tang H Y and Xu X Y 2013 *Chin. Phys. B* **22** 103701
[62] Liu H L, Yin S Q, Liu K K, Qian J, Xu Z, Hong T and Wang Y Z 2013 *Chin. Phys. B* **22** 043701
[63] Liu K K, Zhao R C, Gou W, Fu X H, Liu H L, Yin S Q, Sun J F, Xu Z and Wang Y Z 2016 *Chin. Phys. Lett.* **33** 070602
[64] Zhang Y, Liu Q, Fu X, Sun J, Xu Z and Wang Y 2021 *Opt. Laser Technol.* **139** 106956
[65] Zhang Y, Liu Q X, Sun J F, Xu Z and Wang Y Z 2022 *Chin. Phys. B* **31** 073701
[66] Bardou F, Emile O, Courty J M, Westbrook C I and Aspect A 1992 *Europhys. Lett.* **20** 681
[67] Tol P J J, Herschbach N, Hessels E A, Hogervorst W and Vassen W 1999 *Phys. Rev. A* **60** R761
[68] Shimizu F, Shimizu K and Takuma H 1989 *Phys. Rev. A* **39** 2758
[69] Katori H and Shimizu F 1990 *Jpn. J. Appl. Phys.* **29** L2124
[70] Walhout M, Megens H J L, Witte A and Rolston S L 1993 *Phys. Rev. A* **48** R879
[71] Uhlenberg G, Dirscherl J and Walther H 2000 *Phys. Rev. A* **62** 063404
[72] Brickman K A, Chang M S, Acton M, Chew A, Matsukevich D, Haljan P C, Bagnato V S and Monroe C 2007 *Phys. Rev. A* **76** 043411
[73] Youn S H, Lu M, Ray U and Lev B L 2010 *Phys. Rev. A* **82** 043425
[74] Frisch A, Aikawa K, Mark M, Rietzler A, Schindler J, Zupanič E, Grimm R and Ferlaino F 2012 *Phys. Rev. A* **85** 051401
[75] Miao J, Hostetter J, Stratis G and Saffman M 2014 *Phys. Rev. A* **89** 041401
[76] Maier T, Kadau H, Schmitt M, Griesmaier A and Pfau T 2014 *Opt. Lett.* **39** 3138
[77] Lunden W, Du L, Cantara M, Barral P, Jamison A O and Ketterle W 2020 *Phys. Rev. A* **101** 063403
[78] Miyazawa Y, Inoue R, Matsui H, Takanashi K and Kozuma M 2021 *Phys. Rev. A* **103** 053122
[79] Wang L R, Feng X L, Ma J, Zhao Y T, Xiao L T and Jia S T 2013 *Acta Phys. Sin.* **62** 183301 (in Chinese)
[80] Wen R J, Du J J, Li W F, Li G and Zhang T C 2014 *Acta Phys. Sin.* **63** 244203 (in Chinese)
[81] Essen L and Parry J V L 1955 *Nature* **176** 280
[82] De Beauvoir B, Nez F, Julien L, Cagnac B, Biraben F, Touahri D, Hilico L, Acef O, Clairon A and Zondy J J 1997 *Phys. Rev. Lett.* **78** 440
[83] Knappe S, Shah V, Schwindt P D D, Hollberg L, Kitching J, Liew L A and Moreland J 2004 *Appl. Phys. Lett.* **85** 1460
[84] Laurent Ph, Abgrall M, Jentsch Ch, Lemonde P, Santarelli G, Clairon A, Maksimovic I, Bize S, Salomon Ch, Blonde D, Vega J F, Grosjean O, Picard F, Saccoccio M, Chaubet M, Ladiette N, Guillet L, Zenone I, Delaroche Ch and Sirmain Ch 2006 *Appl. Phys. B* **84** 683
[85] Guena J, Rosenbusch P, Laurent P, Abgrall M, Rovera D, Santarelli G, Tobar M E, Bize S and Clairon A 2010 *IEEE Trans. Ultrason. Ferroelectr. Freq. Control* **57** 647
[86] Hasegawa M, Chutani R K, Gorecki C, Boudot R, Dziuban P, Giordano V, Clatot S and Mauri L 2011 *Sens. Actuators A* **167** 594
[87] Hinkley N, Sherman J A, Phillips N B, Schioppo M, Lemke N D, Beloy K, Pizzocaro M, Oates C W and Ludlow A D 2013 *Science* **341** 1215
[88] Nicholson T L, Campbell S L, Hutson R B, Marti G E, Bloom B J, McNally R L, Zhang W, Barrett M D, Safronova M S, Strouse G F, Tew W L and Ye J 2015 *Nat. Commun.* **6** 6896
[89] Ludlow A D, Boyd M M, Ye J, Peik E and Schmidt P O 2015 *Rev. Mod. Phys.* **87** 637
[90] Liu X, Yudin V I, Taichenachev A V, Kitching J and Donley E A 2017 *Appl. Phys. Lett.* **111** 224102
[91] Liu X, Ivanov E, Yudin V I, Kitching J and Donley E A 2017 *Phys. Rev. Applied* **8** 054001
[92] Hummon M T, Kang S, Bopp D G, Li Q, Westly D A, Kim S, Fredrick C, Diddams S A, Srinivasan K, Aksyuk V and Kitching J E 2018 *Optica* **5** 443
[93] Martin K W, Phelps G, Lemke N D, Bigelow M S, Stuhl B, Wojcik M, Holt M, Coddington I, Bishop M W and Burke J H 2018 *Phys. Rev. Applied* **9** 014019
[94] Liu L, Lü D S, Chen W B, Li T, Qu Q Z, Wang B, Li L, Ren W, Dong Z R, Zhao J B, Xia W B, Zhao X, Ji J W, Ye M F, Sun Y G, Yao Y Y, Song D, Liang Z G, Hu S J, Yu D H, Hou X, Shi W, Zang H G, Xiang J F, Peng X K and Wang Y Z 2018 *Nat. Commun.* **9** 2760
[95] Newman Z L, Maurice V, Drake T, Stone J R, Briles T C, Spencer D T, Fredrick C, Li Q, Westly D, Ilic B R, Shen B, Suh M G, Yang K Y, Johnson C, Johnson D M S, Hollberg L, Vahala K J, Srinivasan K, Diddams S A, Kitching J, Papp S B and Hummon M T 2019 *Optica* **6** 680
[96] Ohmae N, Takamoto M, Takahashi Y, Kokubun M, Araki K, Hinton A, Ushijima I, Muramatsu T, Furumiya T, Sakai Y, Moriya N, Kamiya N, Fujii K, Muramatsu R, Shiimado T and Katori H 2021 *Adv. Quantum Technol.* **4** 2100015
[97] Newman Z L, Maurice V, Fredrick C, Fortier T, Leopardi H, Hollberg L, Diddams S A, Kitching J and Hummon M T 2021 *Opt. Lett.* **46** 4702
[98] Kim K, Aeppli A, Bothwell T and Ye J 2023 *Phys. Rev. Lett.* **130** 113203
[99] Wildermuth S, Hofferberth S, Lesanovsky I, Haller E, Andersson L M, Groth S, Bar-Joseph I, Krüger P and Schmiedmayer J 2005 *Nature* **435** 440
[100] Schwindt P D D, Lindseth B, Knappe S, Shah V, Kitching J and Liew L A 2007 *Appl. Phys. Lett.* **90** 081102
[101] Koschorreck M, Napolitano M, Dubost B and Mitchell M W 2010 *Phys. Rev. Lett.* **104** 093602
[102] Johnson C, Schwindt P D D and Weisend M 2010 *Appl. Phys. Lett.* **97** 243703
[103] Dang H B, Maloof A C and Romalis M V 2010 *Appl. Phys. Lett.* **97** 151110
[104] Behbood N, Martin Ciurana F, Colangelo G, Napolitano M, Mitchell M W and Sewell R J 2013 *Appl. Phys. Lett.* **102** 173504
[105] Holloway C L, Gordon J A, Jefferts S, Schwarzkopf A, Anderson D A, Miller S A, Thaicharoen N and Raithel G 2014 *IEEE Trans. Antennas Propag.* **62** 6169
[106] Grujić Z D, Koss P A, Bison G and Weis A 2015 *Eur. Phys. J. D* **69** 135
[107] McGilligan J P, Griffin P F, Elvin R, Ingleby S J, Riis E and Arnold A S 2017 *Sci. Rep.* **7** 384
[108] Cohen Y, Jadeja K, Sula S, Venturelli M, Deans C, Marmugi L and Renzoni F 2019 *Appl. Phys. Lett.* **114** 073505
[109] Liao K Y, Tu H T, Yang S Z, Chen C J, Liu X H, Liang J, Zhang X D, Yan H and Zhu S L 2020 *Phys. Rev. A* **101** 053432
[110] Hunter D, Dyer T E and Riis E 2022 *Opt. Lett.* **47** 1230
[111] Tayler M C D, Mouloudakis K, Zetter R, Hunter D, Lucivero V G, Bodenstedt S, Parkkonen L and Mitchell M W 2022 *Phys. Rev. Applied* **18** 014036
[112] Kasevich M and Chu S 1991 *Phys. Rev. Lett.* **67** 181
[113] Kasevich M and Chu S 1992 *Appl. Phys. B* **54** 321
[114] Cronin A D, Schmiedmayer J and Pritchard D E 2009 *Rev. Mod. Phys.* **81** 1051
[115] Debs J E, Altin P A, Barter T H, Döring D, Dennis G R, McDonald G, Anderson R P, Close J D and Robins N P 2011 *Phys. Rev. A* **84** 033610
[116] Geiger R, Ménoret V, Stern G, Zahzam N, Cheinet P, Battelier B, Villing A, Moron F, Lours M, Bidel Y, Bresson A, Landragin A and Bouyer P 2011 *Nat. Commun.* **2** 474
[117] Hu Z K, Sun B L, Duan X C, Zhou M K, Chen L L, Zhan S, Zhang Q Z and Luo J 2013 *Phys. Rev. A* **88** 043610

[118] Zhou M K, Duan X C, Chen L L, Luo Q, Xu Y Y and Hu Z K 2015 *Chin. Phys. B* **24** 050401
[119] Kovachy T, Asenbaum P, Overstreet C, Donnelly C A, Dickerson S M, Sugarbaker A, Hogan J M and Kasevich M A 2015 *Nature* **528** 530
[120] Abend S, Gebbe M, Gersemann M, Ahlers H, Müntinga H, Giese E, Gaaloul N, Schubert C, Lämmerzahl C, Ertmer W, Schleich W P and Rasel E M 2016 *Phys. Rev. Lett.* **117** 203003
[121] Hinton A, Perea-Ortiz M, Winch J, *et al.* 2017 *Philos. Trans. R. Soc. Math. Phys. Eng. Sci.* **375** 20160238
[122] Bidel Y, Zahzam N, Blanchard C, Bonnin A, Cadoret M, Bresson A, Rouxel D and Lequentrec-Lalancette M F 2018 *Nat. Commun.* **9** 627
[123] Becker D, Lachmann M D, Seidel S T, *et al.* 2018 *Nature* **562** 391
[124] Bongs K, Holynski M, Vovrosh J, Bouyer P, Condon G, Rasel E, Schubert C, Schleich W P and Roura A 2019 *Nat. Rev. Phys.* **1** 731
[125] Wu X, Pagel Z, Malek B S, Nguyen T H, Zi F, Scheirer D S and Müller H 2019 *Sci. Adv.* **5** eaax0800
[126] Garrido Alzar C L 2019 *AVS Quantum Sci.* **1** 014702
[127] Geiger R, Landragin A, Merlet S and Pereira Dos Santos F 2020 *AVS Quantum Sci.* **2** 024702
[128] Bidel Y, Zahzam N, Bresson A, Blanchard C, Cadoret M, Olesen A V and Forsberg R 2020 *J. Geodesy* **94** 20
[129] Xu R, Li A, Li D and Yan J 2023 *Appl. Sci.* **13** 6076
[130] Carter J D, Cherry O and Martin J D D 2012 *Phys. Rev. A* **86** 053401
[131] Eckel S, Barker D S, Fedchak J A, Klimov N N, Norrgard E, Scherschligt J, Makrides C and Tiesinga E 2018 *Metrologia* **55** S182
[132] Wang C, Xu P, He X D, Wang J and Zhan M S 2012 *Acta Phys. Sin.* **61** 203701 (in Chinese)
[133] Georgescu I M, Ashhab S and Nori F 2014 *Rev. Mod. Phys.* **86** 153
[134] Straatsma C J E, Ivory M K, Duggan J, Ramirez-Serrano J, Anderson D Z and Salim E A 2015 *Opt. Lett.* **40** 3368
[135] Eckel S, Kumar A, Jacobson T, Spielman I B and Campbell G K 2018 *Phys. Rev. X* **8** 021021
[136] Subhankar S, Wang Y, Tsui T C, Rolston S L and Porto J V 2019 *Phys. Rev. X* **9** 021002
[137] Yi C R, Zhang L, Zhang L, Jiao R H, Cheng X C, Wang Z Y, Xu X T, Sun W, Liu X J, Chen S and Pan J W 2019 *Phys. Rev. Lett. 123 190603*
[138] Wang Z Y, Cheng X C, Wang B Z, Zhang J Y, Lu Y H, Yi C R, Niu S, Deng Y, Liu X J, Chen S and Pan J W 2021 *Science* **372** 271
[139] Daley A J, Bloch I, Kokail C, Flannigan S, Pearson N, Troyer M and Zoller P 2022 *Nature* **607** 667
[140] Wang Y, Zhang J H, Li Y, Wu J, Liu W, Mei F, Hu Y, Xiao L, Ma J, Chin C and Jia S 2022 *Phys. Rev. Lett.* **129** 103401
[141] Wang Y, Du H, Li Y, Mei F, Hu Y, Xiao L, Ma J and Jia S 2023 *Light Sci. Appl.* **12** 50
[142] Li Y, Du H, Wang Y, Liang J, Xiao L, Yi W, Ma J and Jia S 2023 *Nat. Commun.* **14** 7560
[143] Briegel H J, Calarco T, Jaksch D, Cirac J I and Zoller P 2000 *J. Mod. Optic.* **47** 415
[144] Saffman M 2016 *J. Phys. B: At. Mol. Opt. Phys.* **49** 202001
[145] Henriet L, Beguin L, Signoles A, Lahaye T, Browaeys A, Reymond G O and Jurczak C 2020 *Quantum* **4** 327
[146] Graham T M, Song Y, Scott J, Poole C, Phuttitarn L, Jooya K, Eichler P, Jiang X, Marra A, Grinkemeyer B, Kwon M, Ebert M, Cherek J, Lichtman M T, Gillette M, Gilbert J, Bowman D, Ballance T, Campbell C, Dahl E D, Crawford O, Blunt N S, Rogers B, Noel T and Saffman M 2022 *Nature* **604** 457
[147] Bluvstein D, Levine H, Semeghini G, Wang T T, Ebadi S, Kalinowski M, Keesling A, Maskara N, Pichler H, Greiner M, Vuletić V and Lukin M D 2022 *Nature* **604** 451
[148] Yu Y, Ma F, Luo X Y, Jing B, Sun P F, Fang R Z, Yang C W, Liu H, Zheng M Y, Xie X P, Zhang W J, You L X, Wang Z, Chen T Y, Zhang Q, Bao X H and Pan J W 2020 *Nature* **578** 240
[149] Duan L M, Lukin M D, Cirac J I and Zoller P 2001 *Nature* **414** 413
[150] Ding D S, Zhang W, Zhou Z Y, Shi S, Xiang G Y, Wang X S, Jiang Y K, Shi B S, Guo G C 2015 *Phys. Rev. Lett.* **114** 050502
[151] Wang Y, Li J, Zhang S, Su K, Zhou Y, Liao K, Du S, Yan H, Zhu S L 2019 *Nat. Photonics* **13** 346
[152] Wen R, Zou C L, Zhu X, Chen P, Ou Z Y, Chen J F and Zhang W 2019 *Phys. Rev. Lett.* **122** 253602
[153] Barker D S, Elgee P K, Sitaram A, Norrgard E B, Klimov N N, Campbell G K and Eckel S 2023 *New J. Phys.* **25** 103046
[154] Riedel M F, Böhi P, Li Y, Hänsch T W, Sinatra A and Treutlein P 2010 *Nature* **464** 1170
[155] Rushton J A, Aldous M and Himsworth M D 2014 *Rev. Sci. Instrum.* **85** 121501
[156] Qu Q, Wang B, Lü D, Zhao J, Ye M, Ren W, Xiang J and Liu L 2015 *Chin. Opt. Lett.* **13** 061405
[157] Keil M, Amit O, Zhou S, Groswasser D, Japha Y and Folman R 2016 *J. Mod. Optic.* **63** 1840
[158] Cheng J, Li X, Zhang J, Xu X, Jiang X, Zhang H and Wang Y 2016 *J. Phys. B: At. Mol. Opt. Phys.* **49** 165301
[159] Rushton J, Roy R, Bateman J and Himsworth M 2016 *New J. Phys.* **18** 113020
[160] Wang X, Song L J, Wang C X, Zhang P F, Li G and Zhang T C 2019 *Chin. Phys. B* **28** 073701
[161] Kim J, Seong J, Yang Y, Moon S W, Badloe T and Rho J 2022 *Adv. Photonics* **4** 024001
[162] Martinez G D, Li C, Staron A, Kitching J, Raman C and McGehee W R 2023 *Nat. Commun.* **14** 3501
[163] Supakar S, Singh V, Tiwari V B and Mishra S R 2023 *J. Appl. Phys.* **134** 024403
[164] Isichenko A, Chauhan N, Bose D, Wang J, Kunz P D and Blumenthal D J 2023 *Nat. Commun.* **14** 3080
[165] Yu Z, Chen L, Duan J, Yao M, Tan N and Liu X 2024 *Appl. Phys. Lett.* **124** 064001
[166] Heine H, Gonidec M S L, Arnold A S, Griffin P F, Riis E, Herr W and Rasel E M 2024 arXiv:2406.10102 [cond-mat.quant-gas]
[167] Zhao Y, Liu X X and Alù A 2014 *J. Opt.* **16** 123001
[168] Khorasaninejad M, Chen W T, Devlin R C, Oh J, Zhu A Y, Capasso F 2016 *Science* **352** 1190
[169] Chang S, Guo X and Ni X 2018 *Annu. Rev. Mater. Res.* **48** 279
[170] Li A, Singh S and Sievenpiper D 2018 *Nanophotonics* **7** 989
[171] Ding F, Yang Y, Deshpande R A and Bozhevolnyi S I 2018 *Nanophotonics* **7** 1129
[172] Bukhari S S, Vardaxoglou J and Whittow W 2019 *Appl. Sci.* **9** 2727
[173] Shen Z and Huang D 2022 *Nanomanufacturing* **2** 194
[174] Yang X, Benelajla M, Carpenter S and Choy J T 2023 *Opt. Express* **31** 13436
[175] Zhou H, Zhao C, He C, Huang L, Man T and Wan Y 2024 *Nanophotonics* **13** 419
[176] Sun S, He Q, Xiao S, Xu Q, Li X and Zhou L 2012 *Nat. Mater.* **11** 426
[177] Kildishev A V, Boltasseva A and Shalaev V M 2013 *Science* **339** 6125
[178] Chen H T, Taylor A J and Yu N 2016 *Rep. Prog. Phys.* **79** 076401
[179] Ding F, Pors A and Bozhevolnyi S I 2017 *Rep. Prog. Phys.* **81** 026401
[180] Genevet P, Capasso F, Aieta F, Khorasaninejad M and Devlin R 2017 *Optica* **4** 139
[181] Hu J, Bandyopadhyay S, Liu Y H and Shao L Y 2021 *Front. Phys.* **8** 586087
[182] Zahra S, Ma L, Wang W, Li J, Chen D, Liu Y, Zhou Y, Li N, Huang Y and Wen G 2021 *Front. Phys.* **8** 593411
[183] Xu Y, Su X, Chai Z and Li J 2023 *Laser Photonics Rev.* **18** 2300355
[184] McClelland J J, Steele A V, Knuffman B, Twedt K A, Schwarzkopf A and Wilson T M 2016 *Appl. Phys. Rev.* **3** 011302
[185] Bergeman T, Erez G and Metcalf H J 1987 *Phys. Rev. A* **35** 1535
[186] Dicke R H 1953 *Phys. Rev.* **89** 472
[187] Schmiedmayer J 1995 *Phys. Rev. A* **52** R13
[188] Denschlag J, Cassettari D, Chenet A, Schneider S and Schmiedmayer J 1999 *Appl. Phys. B* **69** 291
[189] Reichel J, Hänsel W and Hänsch T W 1999 *Phys. Rev. Lett.* **83** 3398
[190] Cassettari D, Chenet A, Folman R, Haase A, Hessmo B, Krüger P, Maier T, Schneider S, Calarco T and Schmiedmayer J 2000 *Appl. Phys. B* **70** 721
[191] Folman R, Krüger P, Cassettari D, Hessmo B, Maier T and Schmiedmayer J 2000 *Phys. Rev. Lett.* **84** 4749
[192] Haase A, Cassettari D, Hessmo B and Schmiedmayer J 2001 *Phys. Rev. A* **64** 043405
[193] Reichel J, Hänsel W, Hommelhoff P and Hänsch T W 2001 *Appl. Phys. B* **72** 81
[194] Günther A, Kemmler M, Kraft S, Vale C J, Zimmermann C and Fortágh J 2005 *Phys. Rev. A* **71** 063619
[195] Fortágh J and Zimmermann C 2007 *Rev. Mod. Phys.* **79** 235
[196] Wildermuth S, Krüger P, Becker C, Brajdic M, Haupt S, Kasper A, Folman R and Schmiedmayer J 2004 *Phys. Rev. A* **69** 030901
[197] Singh V, Tiwari V B and Mishra S R 2020 *Laser Phys. Lett.* **17** 035501

[198] Müller D, Anderson D Z, Grow R J, Schwindt P D D and Cornell E A 1999 *Phys. Rev. Lett.* **83** 5194

[199] Dekker N H, Lee C S, Lorent V, Thywissen J H, Smith S P, Drndić M, Westervelt R M and Prentiss M 2000 *Phys. Rev. Lett.* **84** 1124

[200] Hinds E A, Vale C J and Boshier M G 2001 *Phys. Rev. Lett.* **86** 1462

[201] Thywissen J H, Olshanii M, Zabow G, Drndić M, Johnson K S, Westervelt R M and Prentiss M 1999 *Eur. Phys. J. D* **7** 361

[202] Imhof E, Stuhl B K, Kasch B, Kroese B, Olson S E and Squires M B 2017 *Phys. Rev. A* **96** 033636

[203] Sitaram A, Elgee P K, Campbell G K, Klimov N N, Eckel S and Barker D S 2020 *Rev. Sci. Instrum.* **91** 103202

[204] Seo S, Lee J H, Lee S B, Park S E, Seo M H, Park J, Kwon T Y and Hong H G 2021 *Opt. Express* **29** 35623

[205] Wang G, Xue G, Zhai Q, Zhu J, Yu K, Huang G, Wang M, Zhong A, Zhu L, Yan S and Li X 2021 *Appl. Opt.* **60** 9358

[206] Duan J, Liu X, Zhou Y, Xu X B, Chen L, Zou C L, Zhu Z, Yu Z, Ru N and Qu J 2022 *Opt. Commun.* **513** 128087

[207] Lee K I, Kim J A, Noh H R and Jhe W 1996 *Opt. Lett.* **21** 1177

[208] Pollock S, Cotter J P, Laliotis A, Ramirez-Martinez F and Hinds E A 2011 *New J. Phys.* **13** 043029

[209] Kim J A, Lee K I, Noh H R, Jhe W and Ohtsu M 1997 *Opt. Lett.* **22** 117

[210] Williamson R, Voytas P, Newell R and Walker T 1998 *Opt. Express* **3** 111

[211] Camposeo A, Piombini A, Cervelli F, Tantussi F, Fuso F and Arimondo E 2001 *Opt. Commun.* **200** 231

[212] Bodart Q, Merlet S, Malossi N, Dos Santos F P, Bouyer P and Landragin A 2010 *Appl. Phys. Lett.* **96** 134101

[213] Vangeleyn M, Griffin P F, Riis E and Arnold A S 2009 *Opt. Express* **17** 13601

[214] Vangeleyn M, Griffin P F, Riis E and Arnold A S 2010 *Opt. Lett.* **35** 3453

[215] Lee J, Grover J A, Orozco L A and Rolston S L 2013 *J. Opt. Soc. Am. B* **30** 2869

[216] McGilligan J P, Griffin P F, Riis E and Arnold A S 2015 *Opt. Express* **23** 8948

[217] McGilligan J P, Griffin P F, Riis E and Arnold A S 2016 *J. Opt. Soc. Am. B* **33** 1271

[218] Prikockis M, Wijesinghe H, Chen A, VanCourt J, Roderick D and Sooryakumar R 2016 *Appl. Phys. Lett.* **108** 161106

[219] Cotter J P, McGilligan J P, Griffin P F, Rabey I M, Docherty K, Riis E, Arnold A S and Hinds E A 2016 *Appl. Phys. B* **122** 172

[220] Wang H, Wu H and Shen Z 2017 *Opt. Express* **25** 19609

[221] Bondza S, Lisdat C, Kroker S and Leopold T 2022 *Phys. Rev. Applied* **17** 044002

[222] Burrow O S, Fasano R J, Brand W, Wright M W, Li W, Ludlow A D, Riis E, Griffin P F and Arnold A S 2023 *Opt. Express* **31** 40871

[223] Nshii C C, Vangeleyn M, Cotter J P, Griffin P F, Hinds E A, Ironside C N, See P, Sinclair A G, Riis E and Arnold A S 2013 *Nat. Nanotechnol.* **8** 321

[224] Zhang H, Li T, Yin Y L, Li X J, Xia Y and Yin J P 2016 *Chin. Phys. B* **25** 087802

[225] Chen L, Huang C J, Xu X B, Zhang Y C, Ma D Q, Lu Z T, Wang Z B, Chen G J, Zhang J Z, Tang H X, Dong C H, Liu W, Xiang G Y, Guo G C and Zou C L 2022 *Phys. Rev. Applied* **17** 034031

[226] Bregazzi A, Griffin P F, Arnold A S, Burt D P, Martinez G, Boudot R, Kitching J, Riis E and McGilligan J P 2021 *Appl. Phys. Lett.* **119** 184002

[227] Dyer S, Gallacher K, Hawley U, Bregazzi A, Griffin P F, Arnold A S, Paul D J, Riis E and McGilligan J P 2023 *Phys. Rev. Applied* **19** 044015

[228] Yu Z, Zhu Y, Yao M, Qi F, Chen L, Zou C L, Duan J and Liu X 2024 *Opt. Express* **32** 8919

[229] Vanier J 2005 *Appl. Phys. B* **81** 421

[230] Elvin R, Hoth G W, Wright M, Lewis B, McGilligan J P, Arnold A S, Griffin P F and Riis E 2019 *Opt. Express* **27** 38359

[231] Elvin R, Wright M W, Lewis B, Keliehor B L, Bregazzi A, McGilligan J P, Arnold A S, Griffin P F and Riis E 2020 *Adv. Opt. Technol.* **9** 297

[232] Batori E, Bregazzi A, Lewis B, Griffin F P, Riis E, Mileti G and Affolderbach C 2023 *J. Appl. Phys.* **133** 224401

[233] Lewis B, Elvin R, Arnold A S, Riis E and Griffin P F 2022 *Appl. Phys. Lett.* **121** 164001

[234] Lee J, Ding R, Christensen J, Rosenthal R R, Ison A, Gillund D P, Bossert D, Fuerschbach K H, Kindel W, Finnegan P S, Wendt J R, Gehl M, Kodigala A, McGuinness H, Walker C A, Kemme S A, Lentine A, Biedermann G and Schwindt P D D 2022 *Nat. Commun.* **13** 5131

[235] Barker D S, Norrgard E B, Klimov N N, Fedchak J A, Scherschligt J and Eckel S 2019 *Phys. Rev. Appl.* **11** 064023

[236] Franssen J G H, de Raadt T C H, van Ninhuijs M A W and Luiten O J 2019 *Phys. Rev. Accel. Beams* **22** 023401

[237] McGilligan J P, Moore K R, Dellis A, Martinez G D, de Clercq E, Griffin P F, Arnold A S, Riis E, Boudot R and Kitching J 2020 *Appl. Phys. Lett.* **117** 054001

[238] Ohadi H, Himsworth M, Xuereb A and Freegarde T 2009 *Opt. Express* **17** 23003

[239] Yu N, Genevet P, Kats M A, Aieta F, Tetienne J P, Capasso F and Gaburro Z 2011 *Science* **334** 333

[240] Zhu L, Liu X, Sain B, Wang M, Schlickriede C, Tang Y, Deng J, Li K, Yang J, Holynski M, Zhang S, Zentgraf T, Bongs K, Lien Y H and Li G 2020 *Sci. Adv.* **6** eabb6667

[241] Jin M, Zhang X, Liu X, Liang C, Liu J, Hu Z, Li K, Wang G, Yang J, Zhu L and Li G 2023 *Nano Lett.* **23** 4008

[242] McGehee W R, Zhu W, Barker D S, Westly D, Yulaev A, Klimov N, Agrawal A, Eckel S, Aksyuk V and McClelland J J 2021 *New J. Phys.* **23** 013021

[243] Ropp C, Zhu W, Yulaev A, Westly D, Simelgor G, Rakholia A, Lunden W, Sheredy D, Boyd M M, Papp S, Agrawal A and Aksyuk V 2023 *Light: Sci. Appl.* **12** 83

[244] Dieckmann K, Spreeuw R J C, Weidemüller M and Walraven J T M 1998 *Phys. Rev. A* **58** 3891

[245] Schoser J, Batär A, Löw R, Schweikhard V, Grabowski A, Ovchinnikov Yu B and Pfau T 2002 *Phys. Rev. A* **66** 023410

[246] Dellis A T, Shah V, Donley E A, Knappe S and Kitching J 2016 *Opt. Lett.* **41** 2775

[247] Eriksson S, Trupke M, Powell H F, Sahagun D, Sinclair C D J, Curtis E A, Sauer B E, Hinds E A, Moktadir Z, Gollasch C O and Kraft M 2005 *Eur. Phys. J. D* **35** 135

[248] Yulaev A, Zhu W, Zhang C, Westly D A, Lezec H J, Agrawal A and Aksyuk V 2019 *ACS Photonics* **6** 2902